

MIT Open Access Articles

A Computational Investigation of $\text{Li}_{9}\text{M}_{3}(\text{P}_{2}\text{O}_{7})_{3}(\text{PO}_{4})_{2}$ ($\text{M} = \text{V}, \text{Mo}$) as Cathodes for Li Ion Batteries

The MIT Faculty has made this article openly available. **Please share** how this access benefits you. Your story matters.

Citation: Jain, Anubhav, Geoffroy Hautier, Charles Moore, Byoungwoo Kang, Jinhyuk Lee, Hailong Chen, Nancy Twu, and Gerbrand Ceder. A Computational Investigation of $\text{Li}_{9}\text{M}_{3}(\text{P}_{2}\text{O}_{7})_{3}(\text{PO}_{4})_{2}$ ($\text{M} = \text{V}, \text{Mo}$) as Cathodes for Li Ion Batteries. Journal of The Electrochemical Society 159, no. 5 (2012): A622. ©2012 ECS - The Electrochemical Society

As Published: <http://dx.doi.org/10.1149/2.080205jes>

Publisher: Electrochemical Society

Persistent URL: <http://hdl.handle.net/1721.1/79579>

Version: Final published version: final published article, as it appeared in a journal, conference proceedings, or other formally published context

Terms of Use: Article is made available in accordance with the publisher's policy and may be subject to US copyright law. Please refer to the publisher's site for terms of use.





A Computational Investigation of $\text{Li}_9\text{M}_3(\text{P}_2\text{O}_7)_3(\text{PO}_4)_2$ ($\text{M} = \text{V}, \text{Mo}$) as Cathodes for Li Ion Batteries

Anubhav Jain, Geoffroy Hautier, Charles Moore, Byoungwoo Kang, Jinhyuk Lee, Hailong Chen, Nancy Twu, and Gerbrand Ceder^{*,z}

Massachusetts Institute of Technology, Cambridge Massachusetts 02139, USA

Cathodes with high energy density and safety are sought to improve the performance of Li ion batteries for electric vehicle and consumer electronics applications. In this study, we examine the properties of the potential new cathodes $\text{Li}_9\text{M}_3(\text{P}_2\text{O}_7)_3(\text{PO}_4)_2$ for $\text{M} = \text{V}, \text{Mo}$ with density functional theory calculations. These compounds emerged as potentially interesting cathodes from a high-throughput computational search. In this work, we investigate computationally the voltage, volume change, stability, safety, and diffusivity of $\text{Li}_x\text{V}_3(\text{P}_2\text{O}_7)_3(\text{PO}_4)_2$ and find that extracting the final Li in this material will be difficult due to voltage and safety concerns. We suggest the yet-unreported class of compounds $\text{Li}_x\text{V}_{3-3y}\text{Mo}_{3y}(\text{P}_2\text{O}_7)_3(\text{PO}_4)_2$ as a potential improvement over the pure V compound. In particular, our computations indicate that $y = 2/3$ deserves further computational and experimental attention. © 2012 The Electrochemical Society. [DOI: 10.1149/2.080205jes] All rights reserved.

Manuscript submitted December 21, 2011; revised manuscript received February 16, 2012. Published March 5, 2012.

Li ion batteries are the dominant power source for many consumer electronics, and will for the foreseeable future be the storage technology employed for plug-in hybrid electric vehicles (PHEVs) and electric vehicles (EVs). Improving the performance of Li ion batteries would accelerate adoption of PHEVs and EVs, helping to mitigate concerns over pollution and climate change. One method to improve Li ion battery performance is to design new cathode materials that are safe, cost-effective, and possess a high specific energy and energy density.

Many important properties of cathode materials can now be computed using density functional theory calculations.^{1–3} In particular, operating voltage,⁴ stability, and safety⁵ are relatively simple calculations to automate. The ability to predict many important cathode properties before synthesis makes it possible to rapidly screen cathode materials computationally. We have previously described how such an approach⁶ can lead to the discovery of novel cathode materials.^{7,8}

In this section, we study the compound family $\text{Li}_9\text{M}_3(\text{P}_2\text{O}_7)_3(\text{PO}_4)_2$ with $\text{M} = \{\text{V}, \text{Mo}\}$. The $\text{Li}_9\text{M}_3(\text{P}_2\text{O}_7)_3(\text{PO}_4)_2$ chemistry contains both monophosphate (PO_4) and pyrophosphate (P_2O_7) groups. Monophosphate-based cathodes have been the subject of much investigation since Padhi et al.'s discovery of LiFePO_4 ⁹ and its subsequent characterization as safe^{10–15} and high-rate.^{16–18} Lithium metal pyrophosphates have also been the subject of recent study as cathodes,^{19–21} although they have not been tested as extensively as the monophosphates. Presumably, this is in part because a pyrophosphate group's charge-to-weight ratio is lower than that of a monophosphate group, making it more difficult to achieve high specific energies.²²

The $\text{Li}_9\text{M}_3(\text{P}_2\text{O}_7)_3(\text{PO}_4)_2$ compound family emerged from a high-throughput computational screening procedure whereby we substituted transition metals²³ into all known lithium metal phosphates.²² In particular, a subset of our computations revealed that $\text{M} = \{\text{V}, \text{Mo}\}$ substitution for Fe into $\text{Li}_9\text{Fe}(\text{P}_2\text{O}_7)_3(\text{PO}_4)_2$ was promising for further study. $\text{Li}_9\text{Fe}(\text{P}_2\text{O}_7)_3(\text{PO}_4)_2$ is a known compound that was first reported by Poisson et al. in a non-battery context.²⁴

The vanadium version of this compound, $\text{Li}_9\text{V}_3(\text{P}_2\text{O}_7)_3(\text{PO}_4)_2$, has a theoretical capacity of 173 mAh/g assuming V^{3+} to V^{5+} oxidation. Based on our computational study, it was synthesized experimentally and electrochemically tested by the authors.²⁵ The experimental synthesis and electrochemical characterization of $\text{Li}_9\text{V}_3(\text{P}_2\text{O}_7)_3(\text{PO}_4)_2$ were recently published independently by Kuang et al.²⁶ Subsequently, Xu et al.²⁷ reported on the properties of Cr-doped $\text{Li}_9\text{V}_3(\text{P}_2\text{O}_7)_3(\text{PO}_4)_2$ and Kuang et al. further characterized its charge and discharge behavior.²⁸

In this study, we concentrate on computational results that clarify the electrochemical behavior of $\text{Li}_9\text{V}_3(\text{P}_2\text{O}_7)_3(\text{PO}_4)_2$. In addition,

we investigate replacement of V by Mo as a potential avenue for its improvement. Such a strategy is promising because Mo could theoretically transfer three electrons per formula unit in the $\text{Li}_9\text{Mo}_3(\text{P}_2\text{O}_7)_3(\text{PO}_4)_2$ host. Our computational study finds that substitution of 2/3 of the V site by Mo could lead to higher usable capacity and better intrinsic safety.

Crystal Structure of $\text{Li}_9\text{M}_3(\text{P}_2\text{O}_7)_3(\text{PO}_4)_2$

As reported by Poisson et al.,²⁴ $\text{Li}_9\text{M}_3(\text{P}_2\text{O}_7)_3(\text{PO}_4)_2$ forms in the spacegroup $\text{P}\bar{3}\text{c}1$ and contains alternating anion and cation layers in the c -direction (Figure 1). The anion layers consist of $\text{M}_3(\text{P}_2\text{O}_7)_3(\text{PO}_4)_2$ groups. Each M is octahedrally coordinated: two vertices connect to a single P_2O_7 group, two vertices connect to separate P_2O_7 groups, and the remaining two vertices connect to separate PO_4 groups (a detailed illustration can be found in Poisson et al.).²⁴ The anion layer contains a large in-plane cavity that forms a channel along the c -axis (Figure 1).

The nine lithium ions per formula unit are divided into 3 distinct sites, with occupancies of one, two, and six (Figure 2). Following the notation of Poisson et al.,²⁴ the chemical formula can thus be written as $\text{Li}(1)\text{Li}(2)_2\text{Li}(3)_6\text{V}_3(\text{P}_2\text{O}_7)_3(\text{PO}_4)_2$. The Li(1) sites exhibit an octahedral coordination and are positioned along the channel created by the anion layers, sitting along the c -axis halfway between the anion layers. The Li(2) sites are tetrahedrally coordinated, sit close to the anion layers, and are rotated and stacked along the c -axis (Figure 1). Three vertices of the Li(2) tetrahedron each corner-share with one metal polyhedron and one PO_4 group within the same anion layer. The final vertex corner-shares with a PO_4 group in a different anion layer. The Li(3) sites form strongly distorted tetrahedra (Figure 1) that share one edge with Li(1) and another edge with an MO_6 octahedron. The two vertices that edge-share with the Li(1) site each also corner-share with another Li(3) site and a PO_4 group; these PO_4 groups are in separate anion layers. The two vertices that edge-share with the MO_6 octahedron each also corner-share with a PO_4 group; these PO_4 groups are in the same anion layer.

Methodology

General computational methodology.— For the DFT calculations, we follow the general calculation methodology and parameters outlined in a previous paper.⁶ Our computations employ the GGA functional as parameterized by Perdew et al.²⁹ and were performed using the Vienna Ab Initio Simulation Package.³⁰ We used the rotationally invariant approach to GGA+ U proposed by Dudarev et al.³¹ to correct self-interaction in Mo and V oxides, using $U = 3.1$ for V and $U = 3.5$ for Mo according to the methodology of Wang et al.³² We used a Monkhorst-Pack k -point grid³³ of $2 \times 2 \times 2$ for most calculations

* Electrochemical Society Active Member.

^z E-mail: gceder@mit.edu

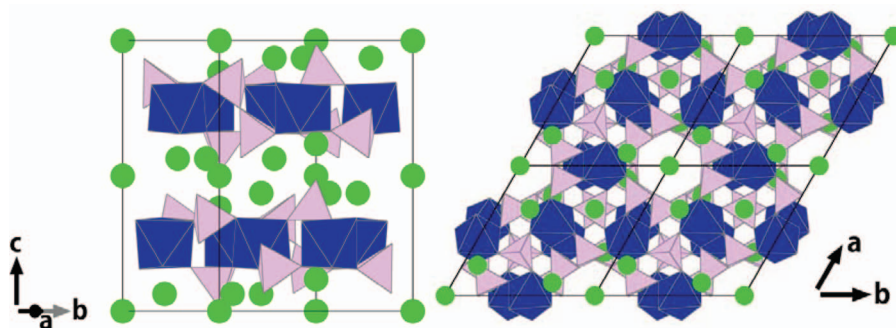


Figure 1. Two views of the $\text{Li}_9\text{V}_3(\text{P}_2\text{O}_7)_3(\text{PO}_4)_2$ structure.⁷⁰ Blue polyhedra represent MO_6 , light purple polyhedra represent PO_4 tetrahedra, and green atoms indicate Li. The drawing on the left demonstrates the alternating layers of Li and $\text{M}_3(\text{P}_2\text{O}_7)_3(\text{PO}_4)_2$ along the c -axis. The drawing on the right, projected along the c -axis, demonstrates the channels created by the anion groups and their occupancy by Li(1) sites (center).

but sometimes increased the mesh to $4 \times 4 \times 2$ to aid in numerical convergence. The magnetic state of all compounds was assumed to be ferromagnetic.

The crystal structures of $\text{Li}_9\text{V}_{3-3y}\text{Mo}_{3y}(\text{P}_2\text{O}_7)_3(\text{PO}_4)_2$ were generated by starting with the positions of the $\text{Li}_9\text{Fe}_3(\text{P}_2\text{O}_7)_3(\text{PO}_4)_2$ crystal structure as reported in the Inorganic Crystal Structure Database (ICSD)^{34,35} and performing two consecutive structural relaxations using the AFLOW software.³⁶ Because Li positions can sometimes be difficult to resolve by X-ray diffraction, we computed the $\text{Li}_9\text{V}_3(\text{P}_2\text{O}_7)_3(\text{PO}_4)_2$ structure starting with slight adjustments to the experimentally-reported Li positions. We calculated 50 structures with the Li starting positions subjected to a random displacement of 0.1–0.2 Å, but did not find a lower-energy ground state.

Many of our calculations involve testing multiple cation orderings to find a ground state. All ground states determined through this procedure were recomputed with electronic and ionic cutoffs tightened by a factor of ten, i.e., electronic cutoff of $n * 5 * 10^{-6}$ eV and ionic cutoff of $n * 5 * 10^{-5}$ eV where n represents the number of atoms in the cell. For these calculations, we expect our total energies to be converged to approximately 10 meV/f.u. (~ 0.2 meV/atom) with respect to electronic and ionic cutoff energy.⁶

$\text{Li}_x\text{V}_3(\text{P}_2\text{O}_7)_3(\text{PO}_4)_2$ convex hull methodology.— For each integer x in $\text{Li}_x\text{V}_3(\text{P}_2\text{O}_7)_3(\text{PO}_4)_2$, we computed the ab initio energy of 100 unique orderings of Li^+ ions³⁷ with the lowest electrostatic energy (as determined by Ewald summation).³⁸ This strategy was first described by Hautier et al.³⁹ For $x = 3$ to $x = 5$, we calculated 25 additional orderings for which we enforced the Li(1) and Li(2) occupancies to be zero. These additional orderings were high in electrostatic energy, but were computed to more thoroughly test which Li arrangement is energetically favorable upon delithiation.

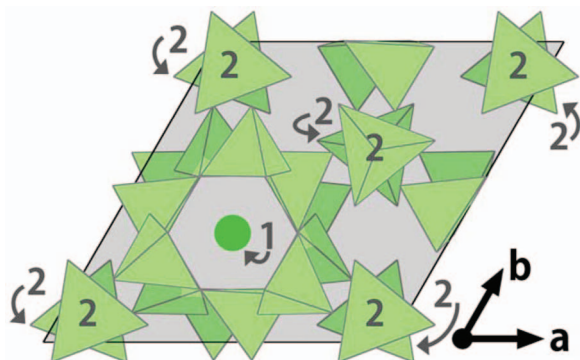


Figure 2. View of Li sites projected along the c -axis.⁷⁰ The Li sites are distributed amongst three positions with occupancies Li(1) = 1, Li(2) = 2, Li(3) = 6. The Li(1) and Li(2) sites are labeled and are stacked and rotated along the c -axis. The Li(3) sites are unlabeled and form 6-member rings by corner sharing. The Li(3) sites also share an edge with the Li(1) sites in the channel. The gray plane along a - b is positioned halfway along the c -axis, directly between the anion layers.

Voltage profiles.— To determine the voltage profiles for the $\text{M} = \text{Mo}$ and $\text{M} = \{\text{Mo}, \text{V}\}$ systems, we did not perform an exhaustive search for the lowest energy Li configurations at intermediate states of delithiation. Instead, we used the lowest-energy Li orderings determined for $\text{Li}_x\text{V}_3(\text{P}_2\text{O}_7)_3(\text{PO}_4)_2$ to compute the voltage profiles for all Mo-doped compounds. For $x < 3$ (for which no V orderings exist), we computed up to 25 Li orderings. Although using the Li orderings determined for $\text{M} = \text{V}$ in the Mo-doped compounds is an approximation, we expect that these orderings will be close in energy to the ground state and will produce reasonably accurate voltage profiles. For the mixed Mo-V compounds, our approximation may be less valid as charge ordering of the metals might more strongly influence cation site energies. However, our assumption is somewhat supported by a previous study from Morgan et al., which demonstrated that similar voltage features occur for pure vanadium NASICON cathodes compared to alloyed NASICON cathodes.⁴⁰

Li-V antisite defect energies.— Vanadium migration upon charging has been linked with irreversible structure changes and capacity loss in layered Li_xVO_2 ⁴¹ and spinel $\text{Li}_x\text{V}_2\text{O}_4$.⁴² As a first step toward investigating whether V migration might play a role in the observed capacity loss^{26,28} for $\text{Li}_x\text{V}_3(\text{P}_2\text{O}_7)_3(\text{PO}_4)_2$, we calculated V-Li antisite defect energies for both fully lithiated and fully delithiated states.

For fully lithiated $\text{Li}_9\text{V}_3(\text{P}_2\text{O}_7)_3(\text{PO}_4)_2$, we started with a 98 atom unit cell and calculated all 108 possible exchanges of one Li site for one V site, i.e., $(\text{Li}_{17}\text{V}_1)(\text{V}_3\text{Li}_1)(\text{P}_2\text{O}_7)_3(\text{PO}_4)_2$. For the delithiated state, we calculated all possible exchanges of Li and V in our ground state ordering for $\text{Li}_3\text{V}_3(\text{P}_2\text{O}_7)_3(\text{PO}_4)_2$, which contains one Li(1) site and two Li(3) sites. We additionally calculated orderings in which we exchanged V with an empty Li(2) site (without affecting Li(1) and Li(3) positions).

Phase Diagrams to Assess Thermodynamic Stability and Safety.— We computed 0 K, 0 atm phase diagrams for Li-V-P-O, Li-Mo-P-O, and Li-V-Mo-P-O using methods described in previous publications.^{43,44} Data was taken from the Materials Project database^{6,45} using crystal structures from the ICSD.^{34,35} We assessed safety by calculating the critical O_2 chemical potential for oxygen release in the charged state according to the methodology outlined by Ong et al.⁵ Oxygen chemical potential ranges for typical binary oxides can be found in the supporting information of Hautier et al.³⁹

We assessed thermodynamic stability of the target compounds by assessing their decomposition energy into known compounds as determined by our phase diagrams. Positive decomposition energies reflect instability of the compound with respect to decomposition; a decomposition energy of zero represents a stable phase.

Diffusion.— We computed migration barriers for Li motion using the Nudged Elastic Band (NEB) method.^{46,47} We used the GGA functional²⁹ (without $+U$) to avoid charge localization and the need to calculate multiple charge orderings for each NEB. Lattice parameters were fixed at the calculated GGA+ U values. All NEB calculations were performed with a single Li vacancy in the primitive cell,

Table I. Calculated and experimental (in parentheses) lattice parameters of the $\text{Li}_9\text{M}_3(\text{P}_2\text{O}_7)_3(\text{PO}_4)_2$ structure. The slight overestimation of the lattice parameter is typical of the GGA+*U* method.

	<i>a</i> (Å)	<i>c</i> (Å)	<i>V</i> (Å ³)
M = Fe ²⁴	9.83 (9.721)	13.73 (13.594)	1148.3 (1112.6)
M = Al ²⁴	9.65 (9.551)	13.60 (13.486)	1096.3 (1065.2)
M = V ^{26,28}	9.88 (9.724, 9.737)	13.73 (13.596, 13.615)	1159.9 (1113.38, 1117.89)
M = Mo	10.00	13.94	1207.3

which contains two formula units and two Li layers as illustrated in Figure 1.

Experimental.— $\text{Li}_9\text{V}_3(\text{P}_2\text{O}_7)_3(\text{PO}_4)_2$ was synthesized by mixing stoichiometric ratios of Li_2CO_3 , $\text{NH}_4\text{H}_2\text{PO}_4$, and V_2O_5 . The powder mixture was ground manually and then dry ball milled in a Paul O. Abbe, Inc., rotary ball mill at 300 RPM for 15 hours. The precursors were pressed into disk-shaped pellets and precalcined at 350° C for 10 hours under a reducing gas mixture of 3% H_2 and 97% Ar. The resulting mixture was re-ground manually using a mortar and pestle, re-pelletized, and subjected to a heat-treatment of 700° C for 10 hours in an environment of 3% H_2 and 97% Ar to produce the desired phase. X-ray characterization was performed using a Rigaku Diffractometer using Cu K α radiation (Figure 5) with 0.02° scanning steps and 3s sample time. Rietveld refinement and profile matching of the powder diffraction data were performed with X'pert HighScorePlus using space group $\text{P}\bar{3}\text{c}1$. Electrochemical tests were performed in a Swagelok style cell using a cathode composed of 80 wt% active material, 15 wt% carbon black, and 5 wt% polytetrafluoroethylene (PTFE) binder mixed using mortar and pestle in an Ar-filled glove box. The total weight of the cathode was approximately 1.83 mg. Lithium metal foil was used as the anode, Celgard 2500 was used as the separator, and 1M LiPF₆ in 1:1 ratio of ethylene carbonate:dimethyl carbonate solution was used as the electrolyte. Electrochemical tests were performed at room temperature in galvanstatic mode on a Maccor 4000 tester at C/10 rate (assuming theoretical capacity of 173 mAh/g) between 2.0 and 4.7 V. Before the first charge, the cell was allowed to rest for 6 hours. All cell tests had 1 minute open-circuit rest at the end of each charge and discharge.

Structure and Stability of $\text{Li}_x\text{M}_3(\text{P}_2\text{O}_7)_3(\text{PO}_4)_2$

The lithiated phases $\text{Li}_9\text{M}_3(\text{P}_2\text{O}_7)_3(\text{PO}_4)_2$.— Table I lists computed and known lattice parameters for M = {Fe, Al, V, and Mo} versions of the $\text{Li}_9\text{M}_3(\text{P}_2\text{O}_7)_3(\text{PO}_4)_2$ structure. Our computed lattice parameters are approximately 0.1 Å–0.2 Å larger than those reported in experiments (regardless of metal), which is typical of the GGA functional. Some of the *c* lattice discrepancy may be attributed to the incomplete description in GGA of van der Waals interactions between layers.

We calculate a density of 2.65 g/cm³ for M = V and 2.92 g/cm³ for M = Mo. The lower theoretical density of the $\text{Li}_9\text{M}_3(\text{P}_2\text{O}_7)_3(\text{PO}_4)_2$ compared with olivine LiFePO₄ (3.49 g/cm³) is expected because the olivine structure has very high density compared to other phosphate structures.²² The lower structural density of the $\text{Li}_9\text{M}_3(\text{P}_2\text{O}_7)_3(\text{PO}_4)_2$ structure leads to a lower theoretical volumetric capacity per electron than LiFePO₄. The theoretical volumetric capacities for $\text{Li}_9\text{V}_3(\text{P}_2\text{O}_7)_3(\text{PO}_4)_2$ (two electrons) and $\text{Li}_9\text{Mo}_3(\text{P}_2\text{O}_7)_3(\text{PO}_4)_2$ (three electrons) are 460 mAh/cm³ and 662 mAh/cm³ compared with 592 mAh/cm³ for LiFePO₄. The high operating voltage of the $\text{Li}_9\text{M}_3(\text{P}_2\text{O}_7)_3(\text{PO}_4)_2$ compounds may partially compensate for its low structural density. We calculate a theoretical specific energy of 1907 Wh/kg and 2803 Wh/kg for $\text{Li}_9\text{V}_3(\text{P}_2\text{O}_7)_3(\text{PO}_4)_2$ and $\text{Li}_9\text{Mo}_3(\text{P}_2\text{O}_7)_3(\text{PO}_4)_2$, respectively, assuming V³⁺ to V⁵⁺ and Mo³⁺ to Mo⁶⁺ oxidation. As a comparison, the theoretical specific energy for LiFePO₄ is 2035 Wh/kg. However, the full theoretical capacity of $\text{Li}_9\text{M}_3(\text{P}_2\text{O}_7)_3(\text{PO}_4)_2$ compounds may not be achievable in practice as

outlined in the Discussion. Likewise, the practical electrode density of LiFePO₄ is severely diminished by the need for carbon coating and nanosizing. The electrode density of $\text{Li}_9\text{M}_3(\text{P}_2\text{O}_7)_3(\text{PO}_4)_2$ may be competitive with or even exceed that of LiFePO₄ if good electrochemical performance can be obtained from large particles or with less conductive carbon. Kuang et al. estimate the electronic conductivity of $\text{Li}_9\text{V}_3(\text{P}_2\text{O}_7)_3(\text{PO}_4)_2$ to be about an order of magnitude higher than that of LiFePO₄.²⁸

We assessed the thermodynamic stability of the lithiated phases by generating Li-V-P-O and Li-Mo-P-O ground state phase diagrams as described in the methodology. The phase diagrams indicate that in the case of both M = V and M = Mo, the reaction competing for stability is:



The calculated reaction energy of 4.1 is −3 meV/atom for M = V and −7 meV/atom for M = Mo, indicating that there is a mild driving force for decomposition. However, it should be noted that the computed values are within typical GGA+*U* errors^{44,48} and also within energy differences caused by finite temperature effects. In previous work, for example, we observed that most phosphate cathodes known to exist experimentally have decomposition energies computed to be less than approximately 10 meV/atom in magnitude.²²

In addition to $\text{Li}_9\text{V}_3(\text{P}_2\text{O}_7)_3(\text{PO}_4)_2$ and $\text{Li}_9\text{Mo}_3(\text{P}_2\text{O}_7)_3(\text{PO}_4)_2$, we also evaluated the energies of the mixed metal compounds $\text{Li}_9\text{V}_{3-3y}\text{Mo}_{3y}(\text{P}_2\text{O}_7)_3(\text{PO}_4)_2$ for *y* = 1/3, 1/2, and 2/3. We calculated all symmetrically distinct orderings of metal substitutions. In all cases, mixing energies are within the convergence limits of our calculations (Table II). Because entropic effects will further stabilize the mixture, our results indicate that a potential Mo/V mixture should not phase separate into $\text{Li}_9\text{V}_3(\text{P}_2\text{O}_7)_3(\text{PO}_4)_2$ and $\text{Li}_9\text{Mo}_3(\text{P}_2\text{O}_7)_3(\text{PO}_4)_2$. However, like their single-metal counterparts, we expect the mixed-metal systems to be mildly unstable (approximately 4–5 meV/atom) with respect to decomposition into Li_3PO_4 , LiVP_2O_7 , and LiMoP_2O_7 . It is plausible that the yet-undiscovered $\text{Li}_9\text{Mo}_3(\text{P}_2\text{O}_7)_3(\text{PO}_4)_2$ and $\text{Li}_9\text{V}_{3-3y}\text{Mo}_{3y}(\text{P}_2\text{O}_7)_3(\text{PO}_4)_2$ could be synthesized.

Structure of delithiated $\text{Li}_{9-x}\text{M}_3(\text{P}_2\text{O}_7)_3(\text{PO}_4)_2$.— To help clarify the observed electrochemical behavior of $\text{Li}_x\text{V}_3(\text{P}_2\text{O}_7)_3(\text{PO}_4)_2$ upon deintercalation,^{26,28} we compute the convex energy hull for $\text{Li}_x\text{V}_3(\text{P}_2\text{O}_7)_3(\text{PO}_4)_2$ according to the methodology described in

Table II. Calculated 0K mixing energies of $\text{Li}_9\text{V}_{3-3y}\text{Mo}_{3y}(\text{P}_2\text{O}_7)_3(\text{PO}_4)_2$ for *y* = 1/3, 1/2, and 2/3. Positive energies indicate unfavorable mixing, but all mixing energies are within the accuracy limits of our calculation⁶ (12 meV/f.u. corresponds to approximately 0.25 meV/atom). Our calculations indicate that there should not be an enthalpic barrier to mixing Mo and V, although there is a mild driving force for decomposition into other solid phases (see text).

<i>y</i> in $\text{Li}_9\text{V}_{3-3y}\text{Mo}_{3y}(\text{P}_2\text{O}_7)_3(\text{PO}_4)_2$	Mixing energy
<i>y</i> = 1/3	1 meV/f.u.
<i>y</i> = 1/2	1 meV/f.u.
<i>y</i> = 2/3	−12 meV/f.u.

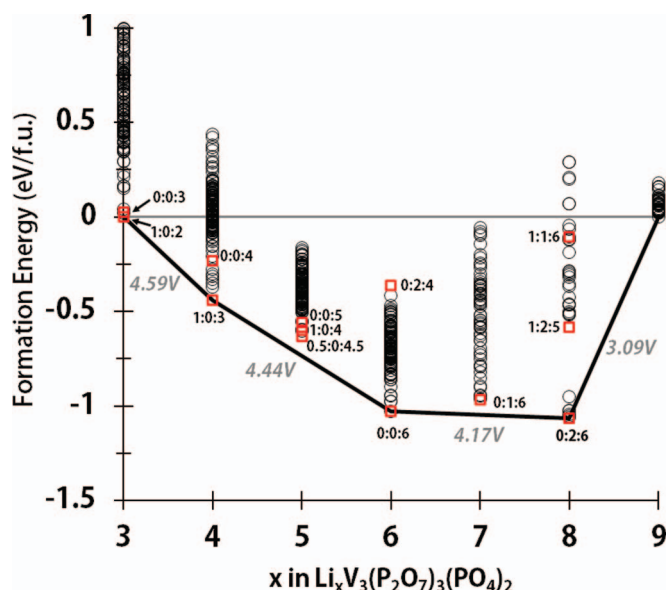


Figure 3. Computed convex hull for $\text{Li}_x\text{V}_3(\text{P}_2\text{O}_7)_3(\text{PO}_4)_2$. Each black circle represents one calculated Li^+ ordering. Voltages computed from the convex hull are indicated in gray text. For selected Li^+ orderings (indicated by red squares), the Li occupancies are indicated by the notation $\text{Li}(1):\text{Li}(2):\text{Li}(3)$.

Section 3.2. The convex hull delineates the lowest energy trajectory as a function of composition and thereby indicates in which order and configuration Li is removed/added during equilibrium deintercalation/intercalation, which is non-obvious in the $\text{Li}_9\text{V}_3(\text{P}_2\text{O}_7)_3(\text{PO}_4)_2$ structure as there exist 3 distinct Li sites. The convex hull can subsequently be used to interpret features in the experimental electrochemical charge-discharge curves.

The computed convex hull is presented in Figure 3. Beginning with the fully lithiated state ($x = 9$), the lowest energy configuration for removing the first Li ($x = 8$) corresponds to removing Li from the Li(1) site in the channel. This configuration is highly favored over removing either the Li(2) or the Li(3) sites: the energy of removing the Li(2) site is 959 meV/Li higher than removing the Li(1) site. It is somewhat difficult to evaluate the energy of removing the Li(3) site as the Li(3) vacancy migrates to the Li(1) position during our structural optimization. We can evaluate the energy for Li(3) removal only by using less stringent ionic convergence parameters; this yields an energy 442 meV/Li higher in energy than removal of Li(1). Our results agree qualitatively with those reported by Kuang et al.²⁸ using similar methods (735 meV greater for Li(2) removal and 489 meV greater for Li(3) removal compared to Li(1) removal); some quantitative disagreement may be attributed to the higher U parameter for V employed by Kuang et al. ($U = 4.0$ compared with $U = 3.1$). We note that in Figure 3, the orderings at $x = 8$ that are close in energy to the ground state (black circles near -1 eV/f.u.) represent supercell orderings where half of the removed Li is from the Li(1) site and the remaining Li is removed from an Li(2) or Li(3) site. The higher energy of the Li(1) site is consistent with the low voltage at which it can be removed.

The $x = 7$ composition is unstable and phase separates into $x = 6$ and $x = 8$ (Figure 3).

At $x = 6$, the lowest energy state corresponds to the Li(1) site and all Li(2) sites removed (Figure 3); only the six Li(3) sites remain in $\text{Li}_6\text{V}_3(\text{P}_2\text{O}_7)_3(\text{PO}_4)_2$. Surprisingly, although we observed the Li(2) site to be much more strongly bound than the Li(3) site when removing a single Li from $\text{Li}_9\text{V}_3(\text{P}_2\text{O}_7)_3(\text{PO}_4)_2$, the Li(2) site is less strongly bound than the Li(3) site when Li is absent from the Li(1) site. This may be due to the edge sharing between the Li(1) octahedra and Li(3) tetrahedra which creates unfavorable electrostatic repulsion when both are occupied.

The $x = 5$ composition is unstable and phase separates into $x = 4$ and $x = 6$ (Figure 3).

At $x = 4$, the lowest energy structure contains one Li(1) site and three Li(3) sites (Figure 3). Our calculations indicate that a Li(3) atom migrates to the Li(1) site when charging from $x = 6$ to $x = 4$, indicating another change in site energetics. As we observed for $x = 8$, reorganization between Li(1) and Li(3) may be facile due to their shared edge. The $x = 4$ ground state provides further evidence that cationic interactions play an important role in the $\text{Li}_9\text{V}_3(\text{P}_2\text{O}_7)_3(\text{PO}_4)_2$ electrochemical profile.

The $x = 3$ state removes an additional Li(3) site; the fully delithiated $\text{Li}_3\text{V}_3(\text{P}_2\text{O}_7)_3(\text{PO}_4)_2$ contains one Li(1) site and two Li(3) sites. However, it should be noted that we find a competing ordering containing three Li(3) sites that is competitive in energy.

In summary, our computations show an ordered state at $x = 8$ due to removal of Li from the Li(1) site; this was initially hypothesized by Xu et al. based on examination of the electrochemical charge/discharge curves²⁷ and recently found computationally by Kuang et al.²⁸ While we compute energetics similar to Kuang et al.²⁸ for removing the first Li site ($\text{Li}(1) \rightarrow \text{Li}(3) \rightarrow \text{Li}(2)$), our detailed study further reveals that these site energetics change as function of Li content. In particular, after removal of the first Li, removal of Li(2) sites become more favorable than removal of Li(3) sites. Were this not the case, the voltage curve would only display two plateaus, corresponding to Li(1) removal followed by removal of five Li(3) sites. Our finding that Li site energetics change with Li content explains why the experimental voltage curve of $\text{Li}_9\text{V}_3(\text{P}_2\text{O}_7)_3(\text{PO}_4)_2$ ^{26,28} displays three voltage plateaus, corresponding to $\text{Li}(1) \rightarrow \text{Li}(2) \rightarrow \text{Li}(3)$ removal.

Lattice parameter changes upon delithiation.— Upon intercalation, the resulting lattice parameter changes can sometimes lead to mechanical fracture of particles, leading to capacity loss on cycling.⁴⁹ A similar effect might be responsible for irreversible capacity loss observed in $\text{Li}_x\text{V}_3(\text{P}_2\text{O}_7)_3(\text{PO}_4)_2$. Therefore, we investigated the change in lattice parameters upon Li removal from $\text{Li}_x\text{V}_3(\text{P}_2\text{O}_7)_3(\text{PO}_4)_2$ and $\text{Li}_x\text{Mo}_3(\text{P}_2\text{O}_7)_3(\text{PO}_4)_2$ (Figure 4).

For $\text{Li}_9\text{V}_3(\text{P}_2\text{O}_7)_3(\text{PO}_4)_2$, we calculate that Li removal always leads to c -lattice parameter increase, whereas the a -lattice parameter decreases or only slightly increases. Our calculations indicate a significant c -lattice expansion of 13.7 Å to 14.6 Å during charge. These calculated results disagree qualitatively with recent experimen-

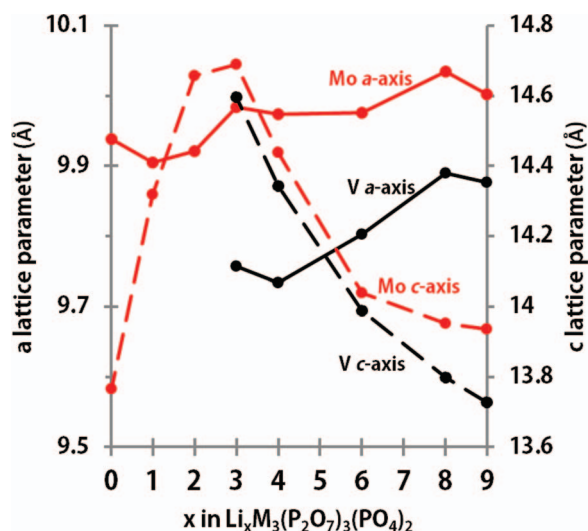


Figure 4. Changes in a - and c -lattice parameters upon Li removal from $\text{Li}_x\text{M}_3(\text{P}_2\text{O}_7)_3(\text{PO}_4)_2$. In general, the a -axis shrinks and the c -axis expands upon delithiation, but the c -axis expansion reverses for $x < 3$. For $x = 4$, the a lattice parameter is plotted as the average of a and b lattice parameters (see text for more details).

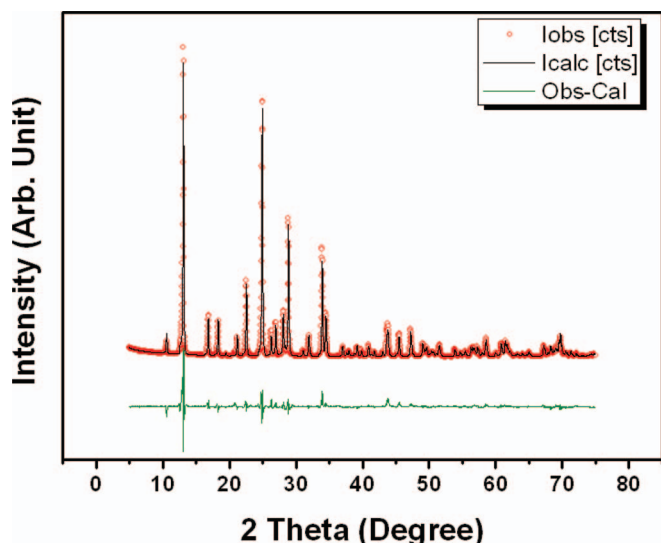


Figure 5. Powder X-ray diffraction pattern of as-synthesized $\text{Li}_9\text{V}_3(\text{P}_2\text{O}_7)_3(\text{PO}_4)_2$.

tal measurements performed by Kuang et al.,²⁸ which indicate that the c -lattice parameter varies only mildly upon charge to $x = 4.1$ (between 13.598 Å and 13.623 Å). In addition, whereas Kuang et al.²⁸ measure the a lattice parameter to always increase upon charge, our calculations indicate both a lattice parameter expansion and contraction upon delithiation.

The discrepancy between computation and experiment for the c -lattice parameter likely stems from the inability of standard GGA functionals to accurately model van der Waals interactions between the layers in the c -axis. Without these interactions, the attraction between the anion layers may be underestimated, leading to overestimation of the c -lattice parameter as is the case in our study. The discrepancy in the calculated a lattice parameter is not as severe as that for the c lattice parameter. From $x = 9$ to $x = 8$, our calculations indicate that the a lattice parameter expands by 0.0125 Å, in good agreement with the results of Kuang et al.,²⁸ which indicate a very slight increase of 0.013 Å. From $x = 8$ to $x = 4$, the calculations indicate that the a lattice parameter contracts, which we speculate is due to V^{3+} being oxidized to the smaller V^{4+} and V^{5+} . From $x = 4$ to $x = 3$, the calculations indicate a slight increase of the a lattice parameter. While the $x = 3$ state should contain only smaller V^{5+} ions, the high valence of +5 might lead to electrostatic repulsion that overcomes ionic size effects. The calculated a lattice parameter trends for $x < 8$ are in slight disagreement with experiments. From $x = 8$ to $x = 7$, the measurements by Kuang et al. indicate that the a lattice parameter slightly increases by 0.039 Å,²⁸ whereas our calculations display a slight decrease of 0.0435 Å. For $x < 7$, comparison between experiment and computation is difficult. There are no measurements by Kuang et al. for $x < 4$, and for $4 < x < 7$

the experiments indicate a two-phase mixture, with the two measured phases having very different a lattice parameters (9.812 Å and 9.439 Å at $x \sim 4$).²⁸ However, it is important to note that despite the individual discrepancies in experimental and computed a and c lattice parameters, the trends in the calculated volume change are still in rough agreement with the experimental data (Table III).

For $x = 4$, our computations indicate that the a and b lattice parameters become inequivalent ($a = 9.771$ Å, $b = 9.697$ Å). At this lithiation level, XRD and HRTEM measurements by Kuang et al.²⁸ indicate the presence of a two-phase mixture. Kuang et al.²⁸ suggest that one of the phases has $\text{P}\bar{3}$ symmetry and contains two unit cells (i.e., 196 atoms), which was not modeled in this work.

For $\text{M} = \text{Mo}$, we evaluated volume changes upon delithiation by using the Li orderings calculated for $\text{M} = \text{V}$. For $x = 9$ to $x = 3$, we calculate similar contractions of the a -lattice parameter and expansion of the c -lattice parameter as for $\text{M} = \text{V}$ (Figure 4). However, it is probable that the lattice parameter trends for $\text{M} = \text{Mo}$ suffer from the same lack of accurate van der Waals characterization as we observed for $\text{M} = \text{V}$. In this case, only trends in calculated cell volumes may be useful, as we found for $\text{M} = \text{V}$.

For $\text{M} = \text{Mo}$, we find that the c -lattice parameter increases with Li extraction for $x > 3$ but decreases with Li extraction for $x < 3$. This calculated behavior is in many respects qualitatively similar to what is observed for the complete deintercalation of LiCoO_2 .⁵⁰ The contraction of the c -lattice parameter at low x may be related to two factors. First, the removal of volume-occupying Li atoms could directly cause c -lattice contraction at low x as was previously hypothesized for LiCoO_2 .⁵¹ Second, the anion layers (which include the transition metal) become more charge-neutral upon Li removal, which could reduce repulsion between layers and thereby reduce the c lattice parameter.

Stability during delithiation.— While we previously observed that the fully lithiated $\text{Li}_9\text{V}_3(\text{P}_2\text{O}_7)_3(\text{PO}_4)_2$ was marginally unstable with respect to the competing reaction 4.1, we find that slightly delithiated $\text{Li}_8\text{V}_3(\text{P}_2\text{O}_7)_3(\text{PO}_4)_2$ is energetically stable. The Li-V-P-O computed phase diagram indicates that the relevant competing reaction for $\text{Li}_8\text{V}_3(\text{P}_2\text{O}_7)_3(\text{PO}_4)_2$ is to $\text{Li}_4\text{P}_2\text{O}_7$, LiVP_2O_7 , $\text{Li}_2\text{V}_2(\text{PO}_4)_3$, and $\text{LiV}_2(\text{PO}_4)_3$, and that the overall energy of decomposition is unfavorable by 5 meV/atom. It is somewhat surprising that our calculations indicate mixed-valent $\text{Li}_8\text{V}_3(\text{P}_2\text{O}_7)_3(\text{PO}_4)_2$ to be a stable phase but the target compound $x = 9$ to be marginally unstable.

As we delithiate further, we find a fairly mild but growing instability (Figure 7). The $x = 6$ state is somewhat unstable (16 meV/atom) against decomposition into $\text{Li}_4\text{P}_2\text{O}_7$, LiPO_3 , and $\text{LiV}_2(\text{PO}_4)_3$. The instability is even higher for $x = 4$ (38 meV/atom) and $x = 3$ (32 meV/atom) with respect to VP_2O_7 , VPO_5 , and LiPO_3 . However, these instability energies are still fairly small.

In contrast to typical LiMO_2 materials, $\text{Li}_9\text{V}_3(\text{P}_2\text{O}_7)_3(\text{PO}_4)_2$ contains residual Li even after fully oxidizing the metal. The residual Li may help retain the structural integrity of the material. The instability of the $\text{M} = \text{Mo}$ compound upon charging is similar to $\text{M} = \text{V}$ for the first six Li removed (Figure 7). However, for the Mo version, full oxidation of the metal would remove all nine Li, i.e.,

Table III. Calculated and experimental²⁸ volumes and volume changes for $\text{Li}_x\text{V}_3(\text{P}_2\text{O}_7)_3(\text{PO}_4)_2$. Our calculations indicate that the $x = 7$ phase is unstable (Figure 3), so we display the average of the $x = 6$ and $x = 8$ volumes. For $x = 4$, the experiments are performed on a slightly Li-rich sample (x closer to 4.1)²⁸ and indicate two different phases. This is discussed in greater detail in the text. Our calculated volume changes with respect to the fully discharged state (in parenthesis) are in rough agreement with experiments despite details of a and c lattice parameter variation being in qualitative disagreement (see text).

composition	calculated volume, Å ³ ($\Delta V/V_i$, %)	experimental volume, ²⁸ Å ³ ($\Delta V/V_i$, %)
$\text{Li}_9\text{V}_3(\text{P}_2\text{O}_7)_3(\text{PO}_4)_2$	1159.91	1117.89
$\text{Li}_8\text{V}_3(\text{P}_2\text{O}_7)_3(\text{PO}_4)_2$	1169.03 (0.79%)	1120.30 (0.22%)
$\text{Li}_7\text{V}_3(\text{P}_2\text{O}_7)_3(\text{PO}_4)_2$	1167.58 (0.66%)	1130.52 (1.13%)
$\text{Li}_4\text{V}_3(\text{P}_2\text{O}_7)_3(\text{PO}_4)_2$	1179.19 (1.66%)	1133.01 (1.35%), 1051.27 (−5.96%)

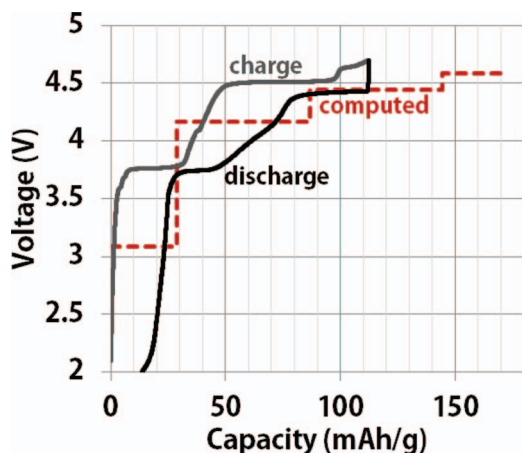


Figure 6. Experimental and computational galvanostatic curves of $\text{Li}_9\text{V}_3(\text{P}_2\text{O}_7)_3(\text{PO}_4)_2$ on first charge and first discharge. The computed voltage profile is derived from the convex hull plotted in Figure 3. Testing was performed at $C/50$.

$\text{Mo}_3(\text{P}_2\text{O}_7)_3(\text{PO}_4)_2$, because Mo can be oxidized to 6+. Removing the final Li in $\text{Li}_x\text{Mo}_3(\text{P}_2\text{O}_7)_3(\text{PO}_4)_2$ causes a spike in the instability reaching approximately 90 meV/atom (Figure 7) with respect to $\text{Mo}(\text{PO}_4)_2$ and P_2O_5 . This magnitude of instability could promote capacity fade due to cathode decomposition to inactive phases during cycling.

Voltage Profiles of $\text{Li}_x\text{M}_3(\text{P}_2\text{O}_7)_3(\text{PO}_4)_2$

Using the methodology outlined by Aydinol et al.⁴ and our convex hull from Figure 3, we are able to compute voltage profiles for $\text{Li}_x\text{M}_3(\text{P}_2\text{O}_7)_3(\text{PO}_4)_2$. We compare our computed results with the experimental data obtained according to the methods described in section 3.7. The cathode sample used for electrochemical testing was confirmed to be single-phase $\text{Li}_9\text{V}_3(\text{P}_2\text{O}_7)_3(\text{PO}_4)_2$ by X-ray diffraction with $R_p = 12.529$ and R_{exp} (R expected) = 3.182.

In Figure 6 the computed voltages are displayed for $M = \text{V}$ alongside the experimentally measured voltage during the first cycle from 2.0 V to 4.7 V. We chose this voltage range because previous studies by Kuang et al.^{26,28} demonstrated that charging to higher than 4.8 V results in a discharge curve that is qualitatively different from the first charge curve.²⁶

The first voltage step (below ~30 mAh/g on charge) represents removal of Li from the Li(1) site. Our computations underestimate the voltage of this step. Whereas the computations predict a voltage of 3.09 V, we measure an experimental charge voltage of 3.65 V. The discharge voltage is closer to our computation (approximately 3.22 V for the final 30 mAh/g shown), but measurements by Kuang et al.²⁸ suggest that the electrode might have slightly changed after completing a charge-discharge cycle. Our calculations are thus overestabilizing $\text{Li}_8\text{V}_3(\text{P}_2\text{O}_7)_3(\text{PO}_4)_2$ relative to $\text{Li}_9\text{V}_3(\text{P}_2\text{O}_7)_3(\text{PO}_4)_2$. Part of the error might be attributed to the fact that our U value, which was calibrated using formation enthalpies for binary vanadium oxides, might be suboptimal for predicting voltages in the $\text{Li}_9\text{M}_3(\text{P}_2\text{O}_7)_3(\text{PO}_4)_2$ crystal structure. A higher value of U would raise the voltage,⁵² and prior work indicates that appropriate U values in phosphates^{52,53} may be higher than those in the oxides.³² Recent calculations by Kuang et al.²⁸ on $\text{Li}_9\text{V}_3(\text{P}_2\text{O}_7)_3(\text{PO}_4)_2$ indeed predict a higher voltage of 3.4 V for the first step using U equal to 4.0. However, it is also possible that the underestimated computed voltage stems from an incomplete understanding of the $\text{Li}_9\text{V}_3(\text{P}_2\text{O}_7)_3(\text{PO}_4)_2$ structure, causing it to be understabilized in our calculation. Although we computed 50 $\text{Li}_9\text{V}_3(\text{P}_2\text{O}_7)_3(\text{PO}_4)_2$ structures with slightly modified lithium positions to try to find an alternate ground state (see Methodology),

we did not find a structure with significantly lower energy than that of the original structure.

Our calculations successfully reproduce the large voltage step between removing the first and second/third Li sites (Figure 6). Our convex hull indicated that this voltage step arises from switching from Li(1) removal to Li(2) removal. Our computed voltage (4.17 V) for the second voltage step is lower than the measured average charge voltage (4.37 V), but closer to the discharge voltage (approximately 4.14 V for the matching step). Our experimental data displays a region of solid solution-like behavior between the first and second plateau that is not reflected in the computation. This might indicate the presence of disorder between Li(1) and Li(2) vacancies. To understand the nature of the solid solution, calculations for $7 < x < 8$ using large supercells may be needed. In addition, subtle effects on the voltage curve often arise from entropic contributions to the free energy that are not modeled in this work. A cluster expansion approach might help reveal the nature of the solid solution.⁵⁴

We calculate an approximately 0.3 V step between removing the third and fourth Li (approximately 87 mAh/g), corresponding to a transition from the $\text{V}^{3+/4+}$ to $\text{V}^{4+/5+}$ redox couple (Figure 6). This calculated voltage step is in agreement with general results obtained from a large number of vanadium phosphates²² but is not present in the experimental curves, either in the present study or previously reported experiments.^{26,28} It is conceivable that there is disproportionation of V^{4+} to V^{3+} and V^{5+} in the material as has been previously suggested for vanadium NASICON cathodes,⁴⁰ although recent XPS data from Kuang et al.²⁸ demonstrates that the oxidation state of V transitions from $3+ \rightarrow 4+ \rightarrow 5+$ during charge. It therefore remains unclear why there is no observable voltage step at approximately 87 mAh/g in the experiments.

At approximately 100 mAh/g, the experimental charge curve exhibits a small voltage step (Figure 6). This step is not predicted by our computations, and is less pronounced in the electrochemical data reported by Kuang et al.²⁶ In addition, the capacity extracted from this step appears to be non-reversible. Therefore, this voltage step may represent a side reaction rather than topotactic removal of Li.

In addition to studying $M = \text{V}$, we also calculated voltage curves for the hypothetical Mo-doped compounds $\text{Li}_x\text{V}_{3-y}\text{Mo}_y(\text{P}_2\text{O}_7)_3(\text{PO}_4)_2$ for $y = 1/3, 1/2, 2/3$, and 1. The full set of calculated voltage curves are presented in Figure 7. For the pure Mo compound ($y = 1$), we note that in theory up to 9 Li^+ may be extracted from the structure as Mo may be oxidized to Mo^{6+} . At $x = 6$, we see only a small voltage step of about 0.1 V corresponding to the transition from the $\text{Mo}^{3+/4+}$ to the $\text{Mo}^{4+/5+}$ redox couple. The small voltage difference between the $\text{Mo}^{3+/4+}$ to $\text{Mo}^{4+/5+}$ redox couples is typical both in phosphates and in oxides.²² Figure 7 also demonstrates a larger voltage step at $x = 3$ of approximately 0.5 V, in line with observations that the $\text{Mo}^{4+/5+}$ and $\text{Mo}^{5+/6+}$ redox couples are approximately 0.3 V apart in phosphates.²² The large final step at $x = 1$ indicates that removing the final Li^+ (from the Li(1) site) leads to an unstable structure. This is also reflected by the sharp increase in the decomposition energy for $x = 0$ (Figure 7).

For the mixed Mo-V compounds, the voltage profile is complex because there exist three distinct Li sites and a total of five active redox couples ($\text{V}^{3+/4+}$, $\text{V}^{4+/5+}$, $\text{Mo}^{3+/4+}$, $\text{Mo}^{4+/5+}$, $\text{Mo}^{5+/6+}$). By analyzing the calculated final magnetic moments on the transition metal ions, we determined that oxidation of the ions in the mixed compounds occurs in the order: $\text{Mo}^{3+/4+}$, $\text{V}^{3+/4+}$, $\text{Mo}^{4+/5+}$, $\text{V}^{4+/5+}$, $\text{Mo}^{5+/6+}$. The order is somewhat surprising as we would have expected $\text{V}^{4+/5+}$ oxidation to occur after $\text{Mo}^{5+/6+}$; data-mined voltages across phosphates demonstrate that the $\text{Mo}^{5+/6+}$ couple in general tends to be approximately 0.4 V lower in voltage than $\text{V}^{4+/5+}$.²² It should be noted that GGA+ U cannot always be relied upon to localize the hole on the appropriate metal, and the order may change depending on the values of U assigned to Mo and V.

Because we expect Mo voltages to be lower than V voltages,²² we also expected that, across the same range of x , the Mo-doped samples would reduce the average voltage from the pure V sample. This is indeed borne out in the calculations; the average voltage from $x = 9$ to $x = 3$ is reduced by 0.1–0.15 V per 1/3 Mo doped (Figure 7). As the

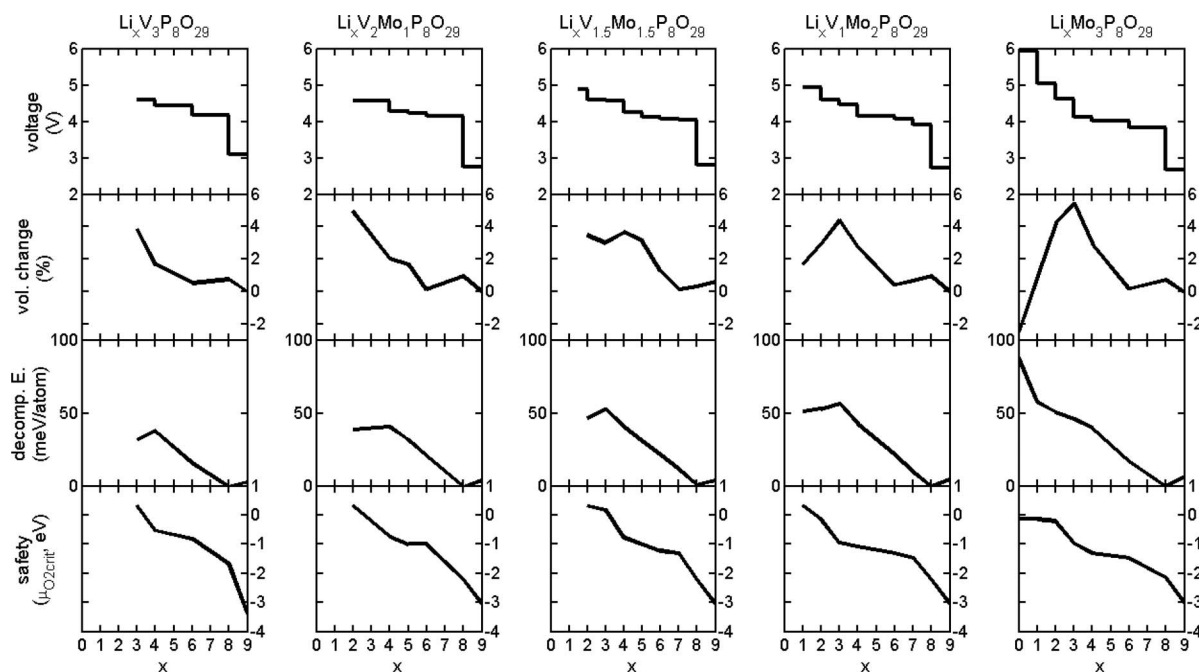


Figure 7. Computed voltage, volume change, thermodynamic decomposition energy, and intrinsic safety with (respect to O_2 release) for the pure metal and mixed metal compounds $Li_xV_{3-3y}Mo_{3y}(P_2O_7)_3(PO_4)_2$ with $y = 0, 1/3, 1/2, 2/3$, and 1.

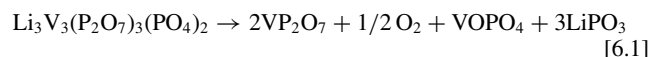
pure V compound is too high in voltage toward the end of charge, we hypothesized that lowering the average voltage might be beneficial for electrochemical performance. However, this advantage is dampened by two factors. First, the Mo doping reduces the voltage of the initial charge step by 0.3–0.4 V due to activation of the $Mo^{3+/4+}$ couple rather than $V^{4+/5+}$. This is undesirable because the initial $V^{4+/5+}$ experimental voltage of 3.75 V is safe and provides good energy density. Second, although Mo doping theoretically increases the capacity due to the possibility of using the Mo^{6+} redox state, it is unclear that this capacity can be fully achieved in practice. Removing the final Li^+ sites (below about $x = 3$) from the Mo-doped materials leads to unstable structures that increase the voltage to over 4.6 V (Figure 7). Therefore, although Mo doping reduces the average voltage, and theoretically may exchange more Li^+ , the capacity near the end of charge may be unusable due to high voltage. We discuss this trade-off in greater detail in the Discussion.

Safety and Stability of the Delithiated Phases

As Li ion batteries become integrated into automotive applications, the issue of safety upon heating becomes of great concern as O_2 released from the cathode can react with the electrolyte to cause thermal runaway. Recently, Ong et al. presented a computational methodology to evaluate the intrinsic safety of Li ion battery cathodes by calculating the critical oxygen chemical potential (μ_{O_2-crit}) at which charged cathodes release O_2 .⁵ In their study, Ong et al. observed that $MnPO_4$ was much more prone to O_2 release (and thereby less safe) than $FePO_4$,⁵ against the intuition of many researchers in the field but in agreement with experimental measurements.^{14,55} Subsequently, Hautier et al. evaluated on a large scale the safety of all interesting battery redox couples in the phosphates chemistry.²² In particular, they observed that V^{5+} and Mo^{6+} have on average a similar μ_{O_2-crit} . Using the same methodology, we evaluated the intrinsic safety of delithiated $Li_3V_3(P_2O_7)_3(PO_4)_2$ and the effect of Mo substitution.

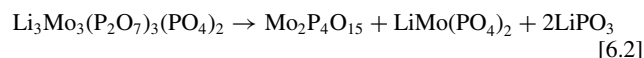
Our calculations indicate that safety is indeed a concern for delithiated $Li_3V_3(P_2O_7)_3(PO_4)_2$, despite the presence of phosphate groups in the structure. Delithiated $Li_3V_3(P_2O_7)_3(PO_4)_2$ is thermodynamically unstable by 32 meV/atom, and its decomposition is predicted to

release O_2 gas according the reaction:



where the O_2 energy has been adjusted for ambient conditions using the correction derived by Wang et al.³² Because fully charged $Li_3V_3(P_2O_7)_3(PO_4)_2$ thermodynamically favors O_2 release, its safety will depend on kinetic limitations to O_2 release rather than a thermodynamic ‘safeguard’. The intrinsic safety concern of this material may limit the ability to reduce particle size to improve electrochemical performance, as smaller particles increase reactivity of the cathode with the electrolyte.

We note that Mo doping improves the safety of $Li_3V_3(P_2O_7)_3(PO_4)_2$. Although delithiated $Li_3Mo_3(P_2O_7)_3(PO_4)_2$ is more thermodynamically unstable (46 meV/atom) than $Li_3V_3(P_2O_7)_3(PO_4)_2$, its decomposition products do not include O_2 gas:



Charged $Li_3Mo_3(P_2O_7)_3(PO_4)_2$ is therefore predicted not to release O_2 under ambient conditions. The μ_{O_2-crit} for oxygen release of $Li_3Mo_3(P_2O_7)_3(PO_4)_2$ is -0.96 , similar to the value we compute for delithiated NASICON $V_2(PO_4)_3$ ($\mu_{O_2-crit} = -1.06$), which has been reported to decompose at approximately 200°C (with the first exothermic peak occurring at 220°C) in the presence of electrolyte.⁵⁶

Fully delithiated $Mo_3(P_2O_7)_3(PO_4)_2$ also is not predicted to release O_2 under ambient conditions, again producing solid reaction products (driving force is 88 meV/atom):



The μ_{O_2-crit} of $Mo_3(P_2O_7)_3(PO_4)_2$ is -0.12 , indicating that its safety should be comparable to charged $Li_{0.5}CoO_2$, which has been reported to decompose between 170 and 230°C.^{57,58} Thus, while the Mo-doped cathodes demonstrate a higher driving force for decomposition in the charged state, the decomposition products are solid phases which are less likely to be of concern for cathode safety.

Table IV. Antisite defect energies (eV) of V exchanged with the given Li site. For $\text{Li}_9\text{V}_3(\text{P}_2\text{O}_7)_3(\text{PO}_4)_2$, no Li(2) sites exist in our equilibrium structure; the calculation marked with an asterisk (*) refers to V^{5+} exchanging with a vacancy on the Li(2) site.

	Li(1)	Li(2)	Li(3)
$\text{Li}_9\text{V}_3(\text{P}_2\text{O}_7)_3(\text{PO}_4)_2$	2.538	1.438	1.891
$\text{Li}_3\text{V}_3(\text{P}_2\text{O}_7)_3(\text{PO}_4)_2$	4.370	4.512*	3.004

Li-V Antisite Defects

When charging to 4.8V, Kuang et al. report that the subsequent discharge of $\text{Li}_9\text{V}_3(\text{P}_2\text{O}_7)_3(\text{PO}_4)_2$ displays different electrochemical behavior. In particular, the discharge voltage drops approximately 0.5 V and voltage plateaus become less pronounced.²⁶ Despite the shift in electrochemistry, Kuang et al.'s initial study does not report any significant changes in the XRD pattern of the cathode before and after charge, indicating that the structural integrity of $\text{Li}_9\text{V}_3(\text{P}_2\text{O}_7)_3(\text{PO}_4)_2$ is maintained.²⁶ A recent follow-up by Kuang et al. indicates that the cell volume differs by 0.36% after charge to 4.6 V and discharge,²⁸ but reports that structural integrity is still maintained. We investigated whether the differences in charge and discharge electrochemical behavior might be due to an exchange of Li and V sites. Such antisite defects could affect the energetics of charging/discharging while perhaps being difficult to detect via XRD.

Table IV lists the calculated antisite defect energies for fully delithiated and fully lithiated $\text{Li}_x\text{V}_3(\text{P}_2\text{O}_7)_3(\text{PO}_4)_2$ in which one Li and one V were exchanged in the 98-atom unit cell. In the lithiated state, the most favorable antisite defect is exchange of V^{3+} with the Li(2) site with energy 1.43 eV. This energy is quite high and should lead to low defect concentrations. In the dilute limit, the defect concentration can be expressed as:

$$c = \frac{N}{V} \exp\left(-\frac{E_F}{kT}\right) \quad [7.1]$$

where c is the defect concentration, N/V is the number of possible defect configurations per unit volume, E_F is the defect formation energy, k is the Boltzmann constant, and T is temperature. For one formula unit of $\text{Li}_9\text{V}_3(\text{P}_2\text{O}_7)_3(\text{PO}_4)_2$, there exist six potential exchanges of Li(2) and V^{3+} sites; using the computed formula unit volume, the defect concentration c would be an extremely low 0.007 cm^{-3} according to equation 7.1. Our calculations thereby suggest that Li-V antisite defects in the fully lithiated phase should not be responsible for changes in electrochemical profile.

In the delithiated state, the defect energies are even higher; the lowest antisite defect energy is approximately 3 eV corresponding to V^{5+} exchange with an Li(3) site. We also calculated the energy of V^{5+} exchanging with an empty Li(2) site, but found this exchange energy to be extremely high (4.5 eV). We did not consider the possibility of Li and V exchange simultaneously accompanied by Li site rearrangement.

Given the extremely high calculated antisite defect energies in the fully charged and fully discharged states (1.43 eV to 4.5 eV), we speculate that the presence of antisite defects is not responsible for the change in the electrochemical profile of $\text{Li}_9\text{V}_3(\text{P}_2\text{O}_7)_3(\text{PO}_4)_2$. However, it should be noted that antisite defects were not investigated for intermediate lithiations, and it cannot be ruled out that the antisite defect energy is more favorable at an intermediate lithium level. It is also possible that other types of defects may be present in this material and further exploration of the defect chemistry of $\text{Li}_9\text{V}_3(\text{P}_2\text{O}_7)_3(\text{PO}_4)_2$ may yield new insights.

Diffusion

Diffusion in $\text{Li}_9\text{V}_3(\text{P}_2\text{O}_7)_3(\text{PO}_4)_2$.— The crystal structure of $\text{Li}_9\text{V}_3(\text{P}_2\text{O}_7)_3(\text{PO}_4)_2$ contains Li-layers and large c-axis channels that contain only Li (Figure 1). A topological depiction of Li sites

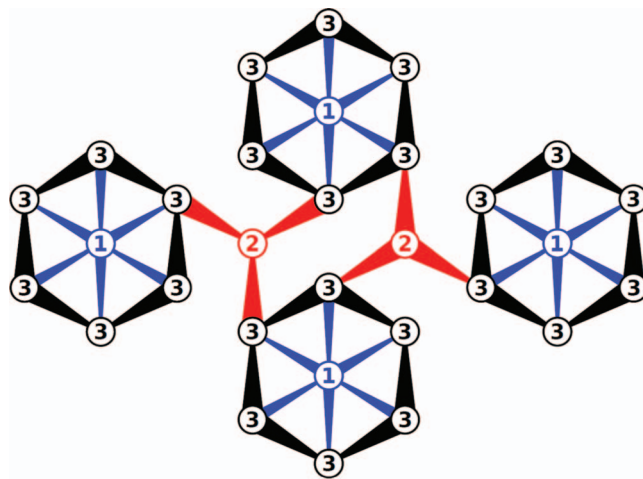


Figure 8. Schematic of in-layer Li diffusion topology (normal to the c-axis). The numbers 1, 2, and 3 represent the Li(1), Li(2), and Li(3) sites, respectively. Connections between sites are drawn with tapered lines to indicate relative displacement of the Li sites above/below the Li layer. Sites and transitions are colored according to symmetry.

and connections between sites within the Li-layer is illustrated in Figure 8. The main features are rings of Li(3) sites with an Li(1) site in the center. The rings are connected to one another via Li(2) sites.

The most obvious pathway for Li diffusion is within the large c-axis channels (between layers). For this pathway, we computed the Li vacancy migration barrier to be 740 meV (Table V), indicating that channel diffusion is likely slow.

An alternate diffusion path for Li is to diffuse across the Li layer. However, both our GGA+ U calculations and our NEB calculations indicate that Li vacancies are not stable at Li(3) sites and relax easily to Li(1) sites. This restricts the number of potential diffusion paths. One plausible diffusion path within the Li layer is a simultaneous $\text{Li}(1) \rightarrow \text{Li}(3)$ and $\text{Li}(3) \rightarrow \text{Li}(2)$ migration of the vacancy so that the vacancy does not rest on an Li(3) site. We calculated the total activation energy of this transition to be extremely large at nearly 1.3 eV (Table V). Much of this net barrier can be traced to the fact that a vacancy in the Li(2) site is thermodynamically much higher in energy than a vacancy in the Li(2) site. The Li(2) site energy compared to the Li(1) site energy is 959 meV higher according to GGA+ U calculations, and 978 meV in the GGA calculations considered here. The net diffusion of Li(1) vacancies to Li(2) sites is largely hindered by the much higher site energy of vacancies in the Li(2) site.

A third potential path for Li(1) vacancy diffusion is a simultaneous hop involving 4 Li ions: $\text{Li}(1) \rightarrow \text{Li}(3)$, $\text{Li}(3) \rightarrow \text{Li}(2)$, $\text{Li}(2) \rightarrow \text{Li}(3)$, and $\text{Li}(3) \rightarrow \text{Li}(1)$. While it appears unlikely that four Li ions are migrating simultaneously, the balance between entering and departing Li from the high-energy Li(1) site may produce a lower net migration barrier. We did not investigate this complex transition in this study.

Diffusion in $\text{Li}_8\text{V}_3(\text{P}_2\text{O}_7)_3(\text{PO}_4)_2$.— We calculated migration barriers in $\text{Li}_8\text{V}_3(\text{P}_2\text{O}_7)_3(\text{PO}_4)_2$ assuming vacancies in all Li(1) sites. Thermodynamically, we expect the Li(2) site to be removed next, as discussed previously. We evaluated several diffusion paths for which the Li(2) vacancy first migrates to the closest Li(3) site, and then migrates to an adjacent Li(3) site. This series of hops is sufficient to form a percolating diffusion network through the Li layer (see Figure 8).

For the first portion of the diffusion path, $\text{Li}(2) \rightarrow \text{Li}(3)$ vacancy migration, we calculated an activation barrier of 518 meV. For the second portion of the diffusion path, $\text{Li}(3) \rightarrow \text{Li}(3)$, migration, we evaluated four different hops. The first hop tested is through the Li channel and crosses Li layers, similar to Li(1) diffusion in the channel. The remaining three hops are illustrated in Figure 9. Each Li(3) site is closely coordinated to three oxygen ions which form a ring around

Table V. Calculated migration barriers for Li vacancy diffusion in $\text{Li}_9\text{V}_3(\text{P}_2\text{O}_7)_3(\text{PO}_4)_2$ and $\text{Li}_8\text{V}_3(\text{P}_2\text{O}_7)_3(\text{PO}_4)_2$. The net activation energy is the energy difference between the activated state and the lowest energy Li-vacancy configuration at the given composition.

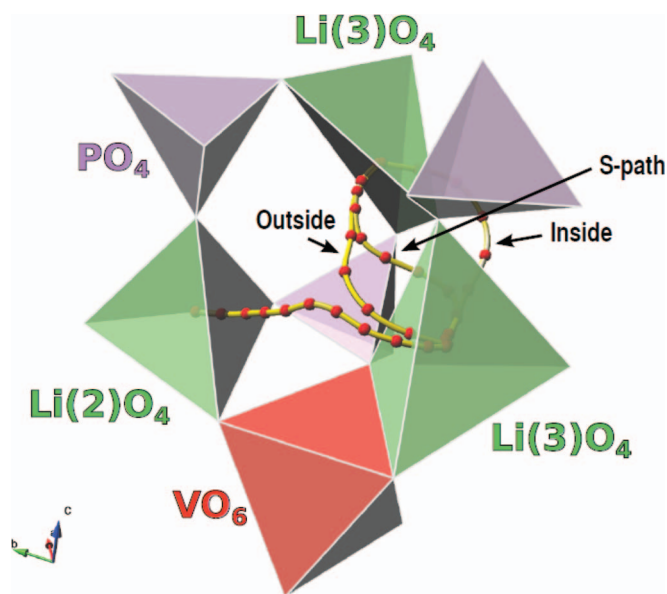
Nominal Composition	Transition		Migration barrier (meV)	Net activation energy (meV)
$\text{Li}_9\text{V}_3(\text{P}_2\text{O}_7)_3(\text{PO}_4)_2$	$\text{Li}(1) \rightarrow \text{Li}(1)$	Between layers	740	740
	$\text{Li}(1) \rightarrow \text{Li}(3)$	Simultaneous	320 (forward)	1291
	$\text{Li}(3) \rightarrow \text{Li}(2)$		1291 (reverse)	
$\text{Li}_8\text{V}_3(\text{P}_2\text{O}_7)_3(\text{PO}_4)_2$	$\text{Li}(2) \rightarrow \text{Li}(3)$		361 (forward)	518
			518 (reverse)	
	$\text{Li}(3) \rightarrow \text{Li}(3)$	Between Layers	1534	1691
		Inside	308	465
		Outside	588	745
		S-route	489	646

the large c-axis channels. The first $\text{Li}(3) \rightarrow \text{Li}(3)$ migration pathway we tested consists of a Li-ion entering into the channel by passing between its neighboring oxygen ions, then exiting the channel via an analogous path ('inside' path). The second pathway consists of traveling around the exterior of the channel ('outside' path). The third pathway follows a S-shape which is interior to the channel near one $\text{Li}(3)$ site and exterior near the other $\text{Li}(3)$ site, transitioning between the two by passing through the oxygen triangle between the $\text{Li}(3)$ site-coordinated oxygen triangles.

For the $\text{Li}(3) \rightarrow \text{Li}(3)$ migration across Li layers, the migration barrier of 1534 meV and net activation energy of 1691 meV are extremely high (Table V). The high migration barrier is not surprising because it essentially involves promoting a $\text{Li}(3)$ vacancy to the $\text{Li}(1)$ site and then $\text{Li}(1)$ vacancy in-channel diffusion. From our results for the fully lithiated case, we can estimate the first part of this migration to be approximately 442 meV and the latter to be 740 meV (Table V).

For the three remaining $\text{Li}(3) \rightarrow \text{Li}(3)$ paths, our calculations indicate that the most favorable transition occurs via the 'inside' path with a low net activation energy of 465 meV (Table V). The S-route and outside migration paths have higher activation energies of 646 meV and 745 meV, respectively.

The energy profile of the migration path from $\text{Li}(2)$ to $\text{Li}(3)$ is plotted in Figure 10. Our results indicate that the rate-limiting step should be the first portion of $\text{Li}(2) \rightarrow \text{Li}(3)$ diffusion with an activation barrier of 518 meV.

**Figure 9.** Diagram showing calculated the $\text{Li}(2) \rightarrow \text{Li}(3)$ hop and the three $\text{Li}(3) \rightarrow \text{Li}(3)$ hops tested (inside, outside, and S-path).

Our calculations on $\text{Li}_9\text{V}_3(\text{P}_2\text{O}_7)_3(\text{PO}_4)_2$ indicate very slow diffusion within the Li-layer (1.3 eV barrier) and faster but still sluggish inter-layer diffusion (740 meV). In contrast, our calculations on $\text{Li}_8\text{V}_3(\text{P}_2\text{O}_7)_3(\text{PO}_4)_2$ indicate reasonably quick diffusion within the Li-layer (518 meV) and very slow inter-layer diffusion (1.7 eV). The discrepancy can be understood simply from the large difference in site energies. When more than 8 Li are present per formula unit, vacancies are only expected on the $\text{Li}(1)$ sites, and in-layer diffusion is sluggish because it requires traversing an $\text{Li}(2)$ site. When fewer than 8 Li are present per formula unit, all $\text{Li}(1)$ sites are vacant and additional vacancies will occupy either $\text{Li}(2)$ or $\text{Li}(3)$ sites. These additional vacancies may move freely within the layer, but inter-layer diffusion is sluggish because it first requires moving a Li from a $\text{Li}(3)$ site into a vacant $\text{Li}(1)$ site.

Our calculations are in reasonable agreement with experimental diffusivity measurements by Poisson et al.²⁴ on the isostructural $\text{Li}_9\text{Al}_3(\text{P}_2\text{O}_7)_3(\text{PO}_4)_2$ and $\text{Li}_9\text{Fe}_3(\text{P}_2\text{O}_7)_3(\text{PO}_4)_2$ where the inter-layer activation barriers were determined to be 1.22 eV and 1.20 eV, respectively, and the in-layer activation barriers were determined to be 660 meV and 690 meV, respectively. Although it is not known whether samples from Poisson et al.²⁴ might have been slightly Li deficient, the activation barriers they report fall between our calculated values for $\text{Li}_8\text{V}_3(\text{P}_2\text{O}_7)_3(\text{PO}_4)_2$ and $\text{Li}_9\text{V}_3(\text{P}_2\text{O}_7)_3(\text{PO}_4)_2$.

The calculated in-plane diffusion activation energy for $\text{Li}_8\text{V}_2(\text{P}_2\text{O}_7)_3(\text{PO}_4)_2$ is higher than some commercialized cathode materials, which have activation barriers of approximately 400 meV or less.^{59–61} However, the higher activation barrier may be partially mitigated by the defect tolerant 2D diffusion network and the large diffusion distance per 518 meV activation (over 9 Å). It would be interesting to investigate the effect of layer spacing on diffusivity as was previously conducted by Kang et al. for the layered oxides.⁶²

Given the large calculated migration barrier for $\text{Li}(1)$ diffusion, it is somewhat surprising that the experimental data reported by Kuang et al. displays only a small overpotential for the $\text{Li}_9\text{V}_2(\text{P}_2\text{O}_7)_3(\text{PO}_4)_2$ to $\text{Li}_8\text{V}_2(\text{P}_2\text{O}_7)_3(\text{PO}_4)_2$ voltage step at a moderate C/10 rate.²⁶ Combined with the evidence that theory underestimates the magnitude of this voltage step, this suggests that the $\text{Li}_9\text{V}_2(\text{P}_2\text{O}_7)_3(\text{PO}_4)_2$ to $\text{Li}_8\text{V}_2(\text{P}_2\text{O}_7)_3(\text{PO}_4)_2$ might involve complicated intercalation behavior that would benefit from further study.

Discussion and Cathode Design

From a design perspective, $\text{Li}_9\text{M}_3(\text{P}_2\text{O}_7)_3(\text{PO}_4)_2$ is a promising cathode for optimization amongst potential phosphate materials. A recent analysis by Hautier et al.²² demonstrates that amongst one-electron phosphates, only chemistries utilizing the $\text{Mn}^{2+/3+}$ and $\text{Cu}^{1+/2+}$ redox couples are capable of surpassing LiFePO_4 's specific energy while retaining a reasonable voltage ($\text{Mn}^{2+/3+}$ in the form of LiMnPO_4 is currently the subject of intense study, and $\text{Cu}^{1+/2+}$ cathodes will likely be difficult to design²²). Beyond the one-electron phosphates, Hautier et al. suggested that the V^{3-5} and Mo^{3-6} redox couples are promising avenues to design phosphates with high specific

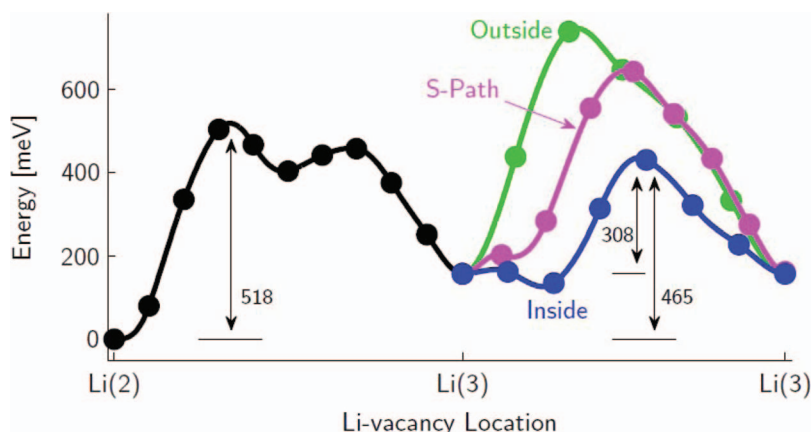


Figure 10. Calculated NEB steps (circles) for $\text{Li}(2) \rightarrow \text{Li}(3)$ migration in the Li layer. The connected lines are cubic spines; the slopes were set based on calculated forces at each image. Three different paths were tested for $\text{Li}(3) \rightarrow \text{Li}(3)$ migration.

energy.²² $\text{Li}_9\text{M}_3(\text{P}_2\text{O}_7)_3(\text{PO}_4)_2$ is an ideal candidate for this latter strategy because it theoretically contains enough Li to support up to three electrons removed per transition metal (the well-studied NASICON $\text{Li}_3\text{M}_2(\text{PO}_4)_3$ is another known example).^{63–65} If both the V^{3-5} and Mo^{3-6} couples could be fully accessed at reasonable voltages, the theoretical capacities of $\text{Li}_9\text{V}_3(\text{P}_2\text{O}_7)_3(\text{PO}_4)_2$ and $\text{Li}_9\text{Mo}(\text{P}_2\text{O}_7)_3(\text{PO}_4)_2$ are 173 mAh/g and 227 mAh/g (compared to 170 mAh/g for LiFePO_4), with the added benefit of a higher operating voltage. Thus, optimization of $\text{Li}_9\text{M}_3(\text{P}_2\text{O}_7)_3(\text{PO}_4)_2$ could be of great commercial interest.

Our computational study of $\text{Li}_9\text{V}_3(\text{P}_2\text{O}_7)_3(\text{PO}_4)_2$ revealed that, in addition to the known problem of high operating voltage,²⁶ a concern for this material is the intrinsic safety of delithiated $\text{Li}_3\text{V}_3(\text{P}_2\text{O}_7)_3(\text{PO}_4)_2$. Although the phosphate chemistry is often assumed to be intrinsically safe due to strong P-O bonds, this assumption has recently been challenged by computational studies^{5,22} and experimental observations.^{66,67} As initially noted by Hautier et al. for phosphates in general,²² O_2 release for $\text{Li}_3\text{V}_3(\text{P}_2\text{O}_7)_3(\text{PO}_4)_2$ is predicted to occur while retaining P-O bonds through reaction 6.1, calling into question the ‘strong P-O bond’ argument and underscoring the need for further computational and experimental investigations of phosphates safety.

The electrochemical data reported by Kuang et al. for $\text{M} = \text{V}$ demonstrate a steady capacity loss on cycling.²⁶ Volume changes during intercalation can sometimes explain capacity loss on cycling due to mechanical fracture of electrode particles.⁴⁹ We calculated that volume changes for $\text{Li}_9\text{V}_3(\text{P}_2\text{O}_7)_3(\text{PO}_4)_2$ were mild (<1.7% up to ~145 mAh/g, <4% for full capacity).

A further reason for capacity loss upon cycling could be decomposition of the active material. Our calculations indicate that decomposition energies of $\text{Li}_9\text{V}_3(\text{P}_2\text{O}_7)_3(\text{PO}_4)_2$ during cycling are generally quite low (<40 meV/atom). Ex-situ analysis of cycled $\text{Li}_9\text{V}_3(\text{P}_2\text{O}_7)_3(\text{PO}_4)_2$ electrodes by Kuang et al.^{26,28} did not find any secondary phases, further suggesting that electrode decomposition is minimal.

Our computed convex hull indicates that Li migrates from the $\text{Li}(3)$ to $\text{Li}(1)$ when charging below $x = 6$, or approximately 87 mAh/g. The electrochemical data from Kuang et al.²⁶ demonstrates that qualitative changes in the discharge curves occur for $\text{Li}_9\text{V}_3(\text{P}_2\text{O}_7)_3(\text{PO}_4)_2$ when charging above approximately 110 mAh/g. It is possible that the change in electrochemical profile is related to the Li migration as was previously suggested for the vanadium NASICON structure⁴⁰ and hypothesized by Kuang et al.²⁶ However, the full mechanism of such a potential structural change remains to be characterized.

We determined that the changes in electrochemical profile when charging to 4.8V²⁶ are likely not caused by antisite defect formation in either the fully lithiated or fully delithiated state. We calculate very high antisite defect formation energies (approximately 1.4 eV for the lithiated state and 3.0 eV for the delithiated state), indicating that antisite defect concentrations are likely very low at the endpoints of lithiation.

Our computations indicate that doping Mo into the V site produces compounds that are only mildly unstable and might therefore be synthesizable. We also hypothesized that such Mo-doping could lower the operating voltage of $\text{Li}_9\text{V}_3(\text{P}_2\text{O}_7)_3(\text{PO}_4)_2$ and additionally provide a higher capacity. Although Mo doping is indeed calculated to lower the average voltage of $\text{Li}_9\text{V}_3(\text{P}_2\text{O}_7)_3(\text{PO}_4)_2$ as was desired, it increases the magnitude of voltage steps during cycling. In particular, the first lithiation step drops by 0.3–0.4 V, making its voltage too low, and the last lithiation step rises close to or above 5 V (Figure 7). The high final voltage step is not intrinsic to the $\text{Mo}^{5+/6+}$ couple but rather due to a high energy needed to extract the final Li^+ sites from the $\text{Li}_9\text{M}_3(\text{P}_2\text{O}_7)_3(\text{PO}_4)_2$ structure. This hypothesis is supported by Figure 7, which demonstrates that the voltage of the last $\text{Mo}^{5+/6+}$ step in Mo-doped samples varies from approximately 4.5 V to approximately 6V depending on the x value at which the Li site is removed. This interpretation is also consistent with data-mined voltages for $\text{Mo}^{5+/6+}$ in phosphates by Hautier et al. that indicate $\text{Mo}^{5+/6+}$ voltages are typically approximately 4 V in the absence of strong Li^+ site effects.²²

The hypothetical Mo-doped samples have slightly higher decomposition energies and slightly higher volume changes than the pure V version (Figure 7). While the decomposition energies of Mo-doped $\text{Li}_9\text{M}_3(\text{P}_2\text{O}_7)_3(\text{PO}_4)_2$ are higher, the decomposition products are solid phases that should lead to better intrinsic safety with respect to O_2 release (Figure 7). The higher values of volume change for Mo-doped compounds may be some cause for concern, but may need to be validated through experimental studies or further computational studies that include explicit van der Waals contributions to the energy.

Although the pure V and pure Mo compounds provide in theory 173 mAh/g and 226 mAh/g of capacity, respectively, it is not clear that the full theoretical capacities can be reversibly and safely attained in practical cells. To evaluate more quantitatively the relative benefits and disadvantages of Mo-doping, we establish several design criteria to be met over the entire intercalation process:

- Voltage must be between 3.0 V and 4.6 V
- Intrinsic safety $\mu_{\text{O}_2\text{-crit}}$ must be less than zero (no thermodynamic driving force for O_2 release under ambient conditions)
- Overall volume change must be under 10%

While these are fairly inclusive criteria, our goal is to allow for some error in the calculations to avoid excluding any potentially promising candidates. We note that an upper cutoff voltage of 4.6 V was the highest voltage demonstrated by Kuang et al. to demonstrate good cyclability.^{26,28}

We present in Table VI the range of x for $\text{Li}_x\text{V}_{3-3y}\text{Mo}_y(\text{P}_2\text{O}_7)_3(\text{PO}_4)_2$ for which each design criterion is met. We then define a ‘usable intercalation range’ by determining the range of x that meet all design criteria. It is important to note that other factors, such as Li^+ diffusivity, may also play a role in determining usable capacity. For this analysis, we have ignored potential diffusion

Table VI. Lithiation ranges for which $\text{Li}_x\text{V}_{3-3y}\text{Mo}_{3y}(\text{P}_2\text{O}_7)_3(\text{PO}_4)_2$ (for $y = 0, 1/3, 1/2, 2/3$, and 1) meet the design criteria specified in the columns. We define a usable intercalation range for each material as the intercalation range that meets all design criteria. We find that only $y = 2/3$ doping expands the usable range of $\text{Li}_x\text{V}_3(\text{P}_2\text{O}_7)_3(\text{PO}_4)_2$.

	Voltage 3.0–4.6 V	Safety $\mu\text{O}_2\text{-crit.} < 0$	Volume Change <10%	Usable range
$\text{Li}_x\text{V}_3(\text{P}_2\text{O}_7)_3(\text{PO}_4)_2$	$x = 9-3$	$x = 9-4$	$x = 9-3$	$x = 9-4$ (5 Li^+) 144 mAh/g 585 Wh/kg
$\text{Li}_x\text{V}_2\text{Mo}_1(\text{P}_2\text{O}_7)_3(\text{PO}_4)_2$	$x = 8-2$	$x = 9-4$	$x = 9-2$	$x = 8-4$ (4 Li^+) 111 mAh/g 466 Wh/kg
$\text{Li}_x\text{V}_{1.5}\text{Mo}_{1.5}(\text{P}_2\text{O}_7)_3(\text{PO}_4)_2$	$x = 8-1.5$	$x = 9-3$	$x = 9-1.5$	$x = 8-3$ (5 Li^+) 135 mAh/g 576 Wh/kg
$\text{Li}_x\text{V}_1\text{Mo}_2(\text{P}_2\text{O}_7)_3(\text{PO}_4)_2$	$x = 8-2$	$x = 9-2$	$x = 9-1$	$x = 8-2$ (6 Li^+) 159 mAh/g 670 Wh/kg
$\text{Li}_x\text{Mo}_3(\text{P}_2\text{O}_7)_3(\text{PO}_4)_2$	$x = 8-3$	$x = 9-0$	$x = 9-0$	$x = 8-3$ (5 Li^+) 127 mAh/g 503 Wh/kg

limitations of the Li(1) site. Therefore, our analysis is meant to represent a ‘best-case’ scenario.

We predict that full capacity will not be reversibly and safely attainable for any of the $\text{Li}_9\text{M}_3(\text{P}_2\text{O}_7)_3(\text{PO}_4)_2$ materials tested. The pure V material, $\text{Li}_9\text{V}_3(\text{P}_2\text{O}_7)_3(\text{PO}_4)_2$, does not meet our criteria for O_2 release at full charge, leading to a ‘best-case’ predicted capacity of 144 mAh/g or 5 Li^+ . High voltage is also a concern for the pure V material as we calculate the last voltage step to be at 4.59 V, and our calculations were observed to slightly underestimate experimental voltages in the high-voltage regime. Thus far, 5 Li^+ has been the maximum capacity of $\text{Li}_9\text{V}_3(\text{P}_2\text{O}_7)_3(\text{PO}_4)_2$ reported in experiments.²⁸

With the exception of $y = 2/3$, our calculations indicate that Mo doping will not expand the number of usable Li that may be extracted from $\text{Li}_x\text{V}_{3-3y}\text{Mo}_{3y}(\text{P}_2\text{O}_7)_3(\text{PO}_4)_2$. For $y = 1/2$ and $y = 1$, predicted voltage and safety concerns limit the usable range to 5 Li^+ , equivalent to the case of $\text{Li}_x\text{V}_3(\text{P}_2\text{O}_7)_3(\text{PO}_4)_2$. However, even if the full usable range of 5 Li^+ could be reversibly extracted from the Mo-doped samples, these materials will exhibit a lower gravimetric and volumetric capacity than their pure V counterpart due to the greater weight of Mo and the larger unit cell of Mo-doped materials (Table VI). They might, however, display other advantages such as a higher diffusivity due to larger lattice parameters of the unit cell.

For $y = 2/3$, we predict that up to 6 Li^+ may be extracted within the guidelines of our design criteria. The capacity over this range is 158.9 mAh/g at an average of 4.2 V, providing an overall theoretical specific energy of approximately 670 Wh/kg (over 10% improvement relative to LiFePO_4). Our calculations indicate that $\text{Li}_9\text{V}_1\text{Mo}_2(\text{P}_2\text{O}_7)_3(\text{PO}_4)_2$ is a promising material for future experimental investigation.

While we studied many aspects of $\text{Li}_9\text{V}_3(\text{P}_2\text{O}_7)_3(\text{PO}_4)_2$, several areas would benefit from further investigation. In particular, further clarifying the diffusion paths and diffusion barriers in this material could yield new ideas for optimization. As one example, tuning the c -lattice parameter to enhance 2D diffusion in layered materials has been investigated previously⁶² and may also be relevant for $\text{Li}_9\text{V}_3(\text{P}_2\text{O}_7)_3(\text{PO}_4)_2$. Finally, while we focused on Mo-doping to reduce voltage, recent computational studies in silicates have suggested N and F doping as a strategy to reduce end-of-charge-voltage. This may be an alternative strategy to apply to $\text{Li}_9\text{V}_3(\text{P}_2\text{O}_7)_3(\text{PO}_4)_2$.^{68,69}

Conclusions

$\text{Li}_9\text{M}_3(\text{P}_2\text{O}_7)_3(\text{PO}_4)_2$ is a new and promising compound family for Li ion battery cathodes suggested by high-throughput computation⁶ which have been successfully synthesized and tested.^{25,26} We present

the first detailed computational investigation of $\text{Li}_9\text{M}_3(\text{P}_2\text{O}_7)_3(\text{PO}_4)_2$ for $\text{M} = \{\text{Mo}, \text{V}\}$. For $\text{M} = \text{V}$, we find that the first voltage step corresponds to Li(1) removal and the second and third steps correspond to Li(2) removal. Further deintercalation leads to removal and rearrangement of the Li(3) and Li(1) sites. We find that the relative energies of the Li(1), Li(2), and Li(3) sites change qualitatively with lithiation level, and that this effect is crucial to predicting the steps in the voltage curve of $\text{Li}_9\text{V}_3(\text{P}_2\text{O}_7)_3(\text{PO}_4)_2$.

For $\text{Li}_9\text{V}_3(\text{P}_2\text{O}_7)_3(\text{PO}_4)_2$, we determined that the experimentally-observed capacity loss upon cycling is likely not the result of cathode decomposition to other phases. In addition, we calculate only small overall volume changes, indicating that mechanical fracture of particles may not be the main cause of capacity loss upon cycling. We concluded that Li vacancy diffusion within the channel should be slow, but diffusion within the layer (assuming Li(1) vacancies) should be moderately fast. Finally, we determined that fully charged $\text{Li}_3\text{V}_3(\text{P}_2\text{O}_7)_3(\text{PO}_4)_2$ may suffer from poor intrinsic safety.

Mo-doping onto the M site should improve the safety of $\text{Li}_9\text{M}_3(\text{P}_2\text{O}_7)_3(\text{PO}_4)_2$, but might lead to detrimental voltage steps during charge/discharge. We determined that a mixture of 2/3 Mo and 1/3 V on the M site could potentially produce a usable specific energy that surpasses that of LiFePO_4 by over 10%. Further investigation of diffusion paths and anion doping might reveal alternate strategies to improve the electrochemical performance of the promising $\text{Li}_9\text{M}_3(\text{P}_2\text{O}_7)_3(\text{PO}_4)_2$ compound family.

Acknowledgments and Funding

The authors thank Robert Doe, Xiaohua Ma, Shyue Ping Ong, and Jae Chul Kim for their efforts on this collaborative project and Robert Daniel for performing preliminary optimization studies of the V-based material. We acknowledge funding from Umicore and Robert Bosch as well as the Department of Energy Basic Energy Sciences under contract #DE-FG02-96ER45571. A. Jain acknowledges funding from the DOE CSGF grant #DE-FG02-97ER25308. This research was supported in part by the National Science Foundation through TeraGrid resources provided by Texas Advanced Computing Center (TACC) under grant number TG-DMR970008S.

References

1. G. Ceder, G. Hautier, A. Jain, and S. P. Ong, *MRS Bulletin*, **36**, 185 (2011).
2. G. Ceder, *MRS Bulletin*, **35**, 693 (2010).

3. Y. S. Meng and M. E. Arroyo-de Dompablo, *Energy & Environmental Science*, **2**, 589 (2009).
4. M. Aydinol, A. Kohan, G. Ceder, K. Cho, and J. Joannopoulos, *Physical Review B*, **56**, 1354 (1997).
5. S. P. Ong, A. Jain, G. Hautier, B. Kang, and G. Ceder, *Electrochemistry Communications*, **12**, 427 (2010).
6. A. Jain, G. Hautier, C. J. Moore, S. Ping Ong, C. C. Fischer, T. Mueller, K. A. Persson, and G. Ceder, *Computational Materials Science*, **50**, 2295 (2011).
7. J. C. Kim, C. J. Moore, B. Kang, G. Hautier, A. Jain, and G. Ceder, *Journal of The Electrochemical Society*, **158**, A309 (2011).
8. G. Hautier, A. Jain, H. Chen, C. Moore, S. P. Ong, and G. Ceder, *Journal of Materials Chemistry*, **21**, 17147 (2011).
9. A. Padhi, K. Nanjundaswamy, and J. Goodenough, *Journal of the Electrochemical Society*, **144**, 1188 (1997).
10. C. Delacourt, P. Poizot, J. M. Tarascon, and C. Masquelier, *Nature materials*, **4**, 254 (2005).
11. D. MacNeil, *Journal of Power Sources*, **108**, 8 (2002).
12. M. Takahashi, *Solid State Ionics*, **148**, 283 (2002).
13. A. Yamada, S. C. Chung, and K. Hinokuna, *J. Electrochem. Soc.*, **148**, A224 (2001).
14. G. Chen and T. J. Richardson, *Journal of Power Sources*, **195**, 1221 (2010).
15. H. F. Xiang, H. Wang, C. H. Chen, X. W. Ge, S. Guo, J. H. Sun, and W. Q. Hu, *Journal of Power Sources*, **191**, 575 (2009).
16. B. Kang and G. Ceder, *Nature*, **458**, 190 (2009).
17. S.-Y. Chung, J. T. Bloking, and Y.-M. Chiang, *Nature materials*, **1**, 123 (2002).
18. D.-H. Kim and J. Kim, *Electrochemical and Solid-State Letters*, **9**, A439 (2006).
19. H. Zhou, S. Upreti, N. A. Chernova, G. Hautier, G. Ceder, and M. S. Whittingham, *Chemistry of Materials*, **23**, 293 (2011).
20. S.-ichi Nishimura, M. Nakamura, R. Natsui, and A. Yamada, *Journal of the American Chemical Society*, **132**, 13596 (2010).
21. A. K. Padhi, K. S. Nanjundaswamy, C. Masquelier, S. Okada, and J. B. Goodenough, *J. Electrochem. Soc.*, **144**, 1609 (1997).
22. G. Hautier, A. Jain, S. P. Ong, B. Kang, C. Moore, R. Doe, and G. Ceder, *Chemistry of Materials*, **23**, 3495 (2011).
23. G. Hautier, C. Fischer, V. Ehrlicher, A. Jain, and G. Ceder, *Inorganic Chemistry*, **50**, 656 (2011).
24. S. Poisson, F. D'Yvoire, H. D. Nguyen, E. Bretey, and P. Berthet, *Journal of solid state chemistry*, **138**, 32 (1998).
25. G. Ceder, A. Jain, G. Hautier, J. C. Kim, and B. W. Kang, U.S. Patent Application No. 12/857,262 (2010).
26. Q. Kuang, J. Xu, Y. Zhao, X. Chen, and L. Chen, *Electrochimica Acta*, **56**, 2201 (2011).
27. J. Xu, Y. Zhao, Q. Kuang, and Y. Dong, *Electrochimica Acta*, **56**, 6562 (2011).
28. Q. Kuang, Z. Lin, Y. Zhao, X. Chen, and L. Chen, *Journal of Materials Chemistry*, **21**, 214760 (2011).
29. J. P. Perdew, K. Burke, and M. Ernzerhof, *Physical Review Letters*, **77**, 3865 (1996).
30. G. Kresse and J. Furthmüller, *Computational Materials Science*, **6**, 15 (1996).
31. S. L. Dudarev, G. A. Botton, S. Y. Savrasov, C. J. Humphreys, and A. P. Sutton, *Physical Review B*, **57**, 1505 (1998).
32. L. Wang, T. Maxisch, and G. Ceder, *Physical Review B*, **73**, 195107 (2006).
33. H. J. Monkhorst and J. D. Pack, *Physical Review B*, **13**, 5188 (1976).
34. G. Bergerhoff, R. Hundt, R. Sievers, and I. Brown, *Journal of Chemical Information and Computer Sciences*, **23**, 66 (1983).
35. Inorganic Crystal Structure Database <http://icsd.fiz-karlsruhe.de/icsd/>.
36. W. Setyawan and S. Curtarolo, *Computational Materials Science*, **49**, 299 (2010).
37. G. Hart and R. Forcade, *Physical Review B*, **80**, 014120 (2009).
38. P. P. Ewald, *Annalen der Physik*, **369**, 253 (1921).
39. G. Hautier, C. C. Fischer, A. Jain, T. Mueller, and G. Ceder, *Chemistry of Materials*, **22**, 3762 (2010).
40. D. Morgan, G. Ceder, Saïdi, J. Barker, J. Swayer, H. Huang, and G. Adamson, *Chemistry of Materials*, **14**, 4684 (2002).
41. L. De Picciotto, M. Thackeray, W. David, P. Bruce, and J. Goodenough, *MRS Bulletin*, **19**, 1497 (1984).
42. G. Pistoia, M. Pasquali, L. A. de Picciotto, and M. M. Thackeray, *Journal of Power Sources*, **34**, 199 (1991).
43. S. Ong, L. Wang, B. Kang, and G. Ceder, *Chemistry of Materials*, **20**, 1798 (2008).
44. A. Jain, G. Hautier, S. P. Ong, C. J. Moore, C. C. Fischer, K. A. Persson, and G. Ceder, *Physical Review B*, **84**, 045115 (2011).
45. Materials Project <http://www.materialsproject.org>.
46. G. Mills and H. Jónsson, *Physical review letters*, **72**, 1124 (1994).
47. H. Jónsson, G. Mills, and K. W. Jacobsen, *Classical and Quantum Dynamics in Condensed Phase Simulations*. (1998).
48. G. Pistoia, S. P. Ong, A. Jain, C. J. Moore, and G. Ceder, *in submission* (2011).
49. H. Wang, Y.-I. Jang, B. Huang, D. R. Sadoway, and Y.-M. Chiang, *Journal of Power Sources*, **81-82**, 594 (1999).
50. G. G. Amatucci, J.-M. Tarascon, and L. C. Klein, *Journal of The Electrochemical Society*, **143**, 1114 (1996).
51. A. Van der Ven, M. Aydinol, G. Ceder, G. Kresse, and J. Hafner, *Physical Review B*, **58**, 2975 (1998).
52. F. Zhou, M. Cococcioni, C. A. Marianetti, D. Morgan, and G. Ceder, *Physical Review B*, **70**, 235121 (2004).
53. F. Zhou, M. Cococcioni, K. Kang, and G. Ceder, *Electrochemistry Communications*, **6**, 1144 (2004).
54. M. Wagemaker, A. Van der Ven, D. Morgan, G. Ceder, F. Mulder, and G. Kearley, *Chemical Physics*, **317**, 130 (2005).
55. S.-W. Kim, J. Kim, H. Gwon, and K. Kang, *Journal of The Electrochemical Society*, **156**, A635 (2009).
56. M. Saïdi, J. Barker, H. Huang, J. L. Swayer, and G. Adamson, *Journal of Power Sources*, **119-121**, 266 (2003).
57. A. Veluchamy, C.-H. Doh, D.-H. Kim, J.-H. Lee, H.-M. Shin, B.-S. Jin, H.-S. Kim, and S.-I. Moon, *Journal of Power Sources*, **189**, 855 (2009).
58. Y. Baba, S. Okada, and J. Yamaki, *Solid State Ionics*, **148**, 311 (2002).
59. A. Van der Ven and G. Ceder, *Journal of Power Sources*, **97-98**, 529 (2001).
60. D. Morgan, A. Van der Ven, and G. Ceder, *Electrochemical and Solid-State Letters*, **7**, A30 (2004).
61. X. Ma, B. Kang, and G. Ceder, *Journal of The Electrochemical Society*, **157**, A925 (2010).
62. K. Kang, Y. S. Meng, J. Bréger, C. P. Grey, and G. Ceder, *Science*, **311**, 977 (2006).
63. K. Nanjundaswamy, A. Padhi, J. Goodenough, S. Okada, H. Ohtsuka, H. Arai, and J. Yamaki, *Solid State Ionics*, **92**, 1 (1996).
64. A. K. Padhi, *Journal of The Electrochemical Society*, **144**, 2581 (1997).
65. M. Manickam, K. Minato, and M. Takata, *Journal of The Electrochemical Society*, **150**, A1085 (2003).
66. G. Chen, X. Song, and T. J. Richardson, *Electrochemical and Solid-State Letters*, **9**, A295 (2006).
67. S.-W. Kim, J. Kim, H. Gwon, and K. Kang, *Journal of The Electrochemical Society*, **156**, A635 (2009).
68. M. Armand, J.-M. Tarascon, and M. E. Arroyo-de Dompablo, *Electrochemistry Communications*, (2011). doi:10.1016/j.elecom.2011.06.027
69. M. Armand and M. E. Arroyo y de Dompablo, *Journal of Materials Chemistry*, (2011). doi:10.1039/c0jm04216a
70. K. Momma and F. Izumi, *Journal of Applied Crystallography*, **41**, 653 (2008).